NATIONAL AERONAUTICS AND SPACE ADMINISTRATION

Space Programs Summary No. 37-35, Volume VI

for the period July 1, 1965 to August 31, 1965

Space Exploration Programs and Space Sciences

JET PROPULSION LABORATORY
CALIFORNIA INSTITUTE OF TECHNOLOGY
PASADENA, CALIFORNIA

September 30, 1965

NATIONAL AERONAUTICS AND SPACE ADMINISTRATION

Space Programs Summary No. 37-35, Volume VI

for the period July 1, 1965 to August 31, 1965

Space Exploration Programs and Space Sciences

JET PROPULSION LABORATORY
CALIFORNIA INSTITUTE OF TECHNOLOGY
PASADENA, CALIFORNIA

September 30, 1965

Preface

The *Space Programs Summary* is a six-volume, bimonthly publication that documents the current project activities and supporting research and advanced development efforts conducted or managed by JPL for the NASA space exploration programs. The titles of all volumes of the *Space Programs Summary* are:

Vol. I. The Lunar Program (Confidential)

Vol. II. The Planetary–Interplanetary Program (Confidential)

Vol. III. The Deep Space Network (Unclassified)

Vol. IV. Supporting Research and Advanced Development (Unclassified)

Vol. V. Supporting Research and Advanced Development (Confidential)

Vol. VI. Space Exploration Programs and Space Sciences (Unclassified)

The *Space Programs Summary,* Vol. VI consists of an unclassified digest of appropriate material from Vols. I, II, and III; an original presentation of technical supporting activities, including engineering development of environmental-test facilities, and quality assurance and reliability; and a reprint of the space science instrumentation studies of Vols. I and II. This instrumentation work is conducted by the JPL Space Sciences Division and also by individuals of various colleges, universities, and other organizations. All such projects are supported by the Laboratory and are concerned with the development of instruments for use in the NASA space flight programs.

W. H. Pickering, *Director*
Jet Propulsion Laboratory

Space Programs Summary No. 37-35, Vol. VI

Prepared under Contract No. NAS 7-100, National Aeronautics & Space Administration

Contents

LUNAR PROGRAM

I. *Surveyor* Project 1
A. Introduction 1
B. Systems Testing 1
C. Flight Control 3
D. Electronics 3
E. Electrical Power Supply 3
F. Scientific Payload 5
G. Propulsion 5
H. Test Facilities and Equipment 6

PLANETARY–INTERPLANETARY PROGRAM

II. *Mariner* Project 9
A. Introduction 9
B. *Mariner IV* Space Flight Operations 10
C. *Mariner IV* Spacecraft Performance During the Mission . . . 10
D. Future Operations for *Mariner IV* 12

DEEP SPACE NETWORK

III. Deep Space Instrumentation Facility 13
A. Introduction 13
B. Tracking Stations Engineering and Operations 13
C. Developmental and Testing Activities 17

IV. Space Flight Operations Facility 21
A. Introduction 21
B. Simulation Data Conversion Center 21
C. *Mariner* Master Data Library 22

SUPPORTING ACTIVITIES

V. Environmental Test Facilities 23
A. Six-Channel Automatic Accelerometer Selector 23

Contents (Cont'd)

SPACE SCIENCES

VI. Space Instruments 29

A. Preparations for the Analysis of *Surveyor* Video Data 29

B. Planetary Color Photography 31

VII. Physics 35

A. Total Radiation Dose Experienced by the *Mariner IV* Spacecraft as Measured by the Ion Chamber Experiment 35

B. *Mariner IV* Magnetic Measurements Inside the Earth's Magnetosphere, Magnetic Tail, and Magnetosheath 37

References 44

LUNAR PROGRAM

I. *Surveyor* Project

A. Introduction

Calculated to span the gap between the *Ranger* Project and Project *Apollo*, the *Surveyor* Project is designed to take the next step in advancing lunar technology by making soft landings on the Moon with unmanned spacecraft. Various engineering and scientific experiments will be performed during touchdown and while on the lunar surface. The first launches will be engineering test missions to demonstrate system capability up to soft landing and limited postlanding operations. The engineering payload includes elements of redundancy, diagnostic telemetry, touchdown instrumentation, and survey TV.

Following the engineering test missions, the objectives are to extend our knowledge of lunar conditions and to verify the suitability of *Apollo* landing sites. The science payload is planned to consist of two-camera TV, micrometeorite ejecta, single-axis seismometer, alpha particle scattering, soil mechanics surface sampler, and touchdown dynamics experiments.

Hughes Aircraft Company (HAC), Space Systems Division, is under contract to develop and fabricate the first seven spacecraft. The JPL Space Flight Operations Facility and the Deep Space Network (Mission Operations System) will be utilized for flight control and tracking. The first flight, using an *Atlas/Centaur* launch vehicle, is scheduled for late-1965.

B. Systems Testing

1. SC-1 Flight Spacecraft

A special RF-link phase jitter test was performed on the SC-1 flight spacecraft at HAC during this reporting period. The purpose was to demonstrate that phase lock could be maintained during vibration of the spacecraft omni-antenna with an RF link established between the system test equipment assembly transmitter and the spacecraft receiver–transmitter. Preliminary review of the test results shows that a satisfactory RF link was obtained, and no appreciable phase jitter was introduced.

Vibration testing was also performed as part of the flight-acceptance test program for the SC-1 spacecraft.

Results indicate that the functional operation of the spacecraft was not degraded during the vibration environment. Vibration characteristics were within specification requirements, except for certain deviations which were jointly assessed by HAC and JPL during the operation as being acceptable and not necessitating retest.

Other special tests are being performed to supply additional confidence in the functional performance of the vehicle. Thus far, except for a few minor problems which are being investigated, the operation of the SC-1 spacecraft has been satisfactory.

2. SC-2 Flight Spacecraft

The SC-2 flight spacecraft was being upgraded throughout the entire reporting period, and no system tests were performed. Units for SC-2 not previously group-tested and units previously group-tested which had failures, out-of-tolerance data, or significant modifications were again group-tested on the Group Test 1 vehicle. Following upgrade, SC-2 will be subjected to new and more extensive power and grounding checks and will then begin initial system checkout tests with System Test Equipment Assembly 4.

3. Group Test 1 (GT-1) Vehicle

The GT-1 vehicle has been used to support group testing for SC-2, SC-3, and SP-1 (flight-quality spare subsystem set), to investigate problems arising from SC-1 system testing, and to verify proposed SC-1 modifications. When SC-2 completes upgrading operations, GT-1 will be removed from System Test Equipment Assembly 4 and will then begin a short upgrade program.

4. T-2N-1 Descent Dynamics Test Vehicle

System testing of the T-2N-1 vehicle was completed, and the vehicle was shipped to the Air Force Missile Development Center. Weight, balance, and alignment checks and functional tests were performed in preparation for the first operating test of the vehicle while tethered from a balloon.

5. T-2N-R Recovery System Test Vehicle

The T-2N-R vehicle has been tested four times in drops from a balloon, and recovery provisions have performed satisfactorily. Two additional tests will be made.

6. T-21 Prototype System Test Spacecraft

The T-21 spacecraft was put through the Pathfinder Mission at the Eastern Test Range (ETR) during this reporting period. (Pathfinder denotes the exploratory nature of the mission, utilizing schedules, procedures, operations, personnel, and equipment previously untried in the ETR environment.) The mission consisted of seven phases: (1) receipt, partial assembly, and electronics testing; (2) propellant loading; (3) final assembly, weight and balance checks, optical alignment, and encapsulation; (4) spacecraft mating to the *Centaur* simulator and system readiness and countdown tests; (5) decapsulation and partial disassembly; (6) propellant downloading; and (7) preparation for shipment. The Pathfinder Mission was successful in that it exposed many areas that would have hindered ETR operations on the SC-1 flight spacecraft.

After the completion of the mission, T-21 was prepared for shipment to the Goldstone Pioneer Station for mission operations testing. The primary objective of these tests is to demonstrate the engineering and functional

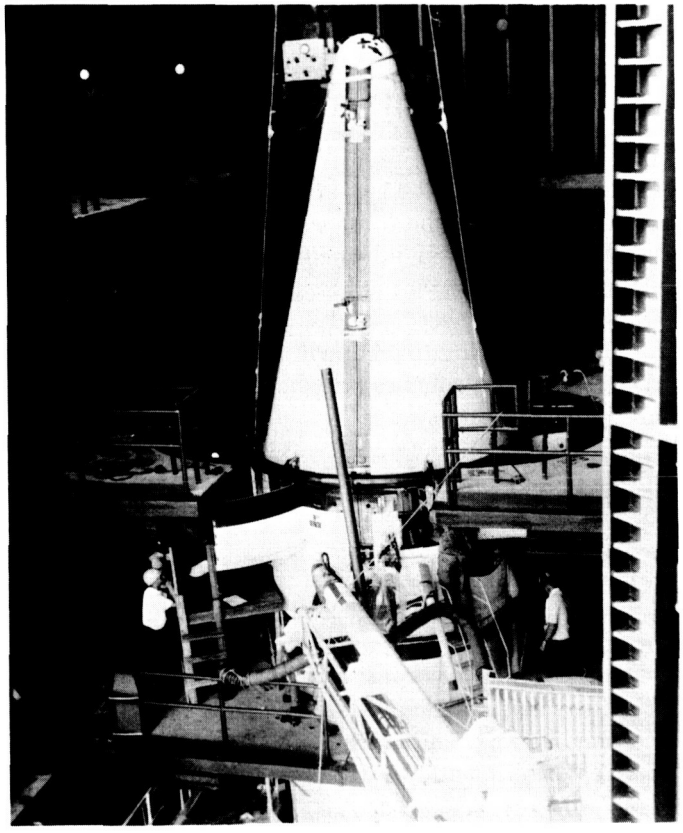

Fig. 1. SD-2 model mated to the *Atlas/Centaur* 6 launch vehicle

compatibility between an actual flight-equivalent spacecraft and the *Surveyor* JPL Space Flight Operations Facility/Deep Space Network system and to provide operational training for the respective personnel. The secondary objective is to establish the validity of spacecraft simulation techniques.

7. SD-2 Spacecraft Dynamic Model

At the beginning of the reporting period, the SD-2 model was in the Explosive Safe Facility at the ETR, assembled and checked out. After encapsulation and a simulated countdown, SD-2 was moved to the launch pad and mated to the *Atlas/Centaur 6* launch vehicle (Fig. 1). A tanking test and a special test to determine the results of random umbilical pulling have been performed. The SD-2 model remains in a "go" condition, awaiting the joint flight-acceptance composite tests, shortly after which testing will be completed. All test delays have resulted from causes other than SD-2 readiness.

C. Flight Control

A prototype model of the new Canopus sensor shade design has passed the required type-approval levels of vibration. The new configuration includes a greater number of baffles than the previous shade tested. The center-of-gravity and mass moment of this new shade indicate more desirable dynamic characteristics than those of the current production model. Tests to determine the effects of reflected light from the lunar surface and reflected sunlight from nearby spacecraft structures (such as those performed on the developmental model; see *SPS 37-34*, Vol. VI, p. 16) will be performed using the new design. The results of these tests should verify that this shade's performance is equal to or better than that of the developmental shade evaluated previously.

D. Electronics

1. Low-Gain Upper-Hemispherical Antenna

Consideration is being given to the addition of another antenna on the spacecraft to improve the over-all performance of the telecommunications subsystem, and development work has begun. Having a broad pencil beam and a small backlobe, this antenna would be mounted above the spacecraft, with the peak gain in the spacecraft $-z$ direction. The antenna would have right elliptical polarization and operate at both transmit and receive frequencies. The patterns would be influenced by the spacecraft to a much lesser degree than the patterns of the present omni-antennas because of the much smaller backlobe radiation of this low-gain antenna. Also, a significant reduction of the lunar reflection problem should be realized.

2. Auxiliary Antenna Switch

The design effort is nearing completion for an auxiliary antenna switch to select between the upper-hemispherical antenna and the omni-antenna. The switch assembly will be comprised of a single-pull double-throw RF switch and solid-state drive circuitry to actuate the switch. The operation of the unit will be the same as that of the transfer switch, and the same associated drive circuitry in the transmitter will be utilized.

E. Electrical Power Supply

Since a solar eclipse will subject a solar panel to rapid temperature changes, tests were run in the HAC solar-thermal-vacuum chamber to determine the maximum temperature rate of change and to verify that the *Surveyor* panel will be able to withstand the thermal shock. The thermal test consisted of two exposures representing: (1) a ½-hr eclipse, which is the maximum spacecraft eclipse time; and (2) the 1-hr period during which the spacecraft may be randomly oriented while the solar panel is shadowed. In both exposures, in the cooldown from 143°F (maximum transit temperature), the solar panel temperature dropped 33°F in the first minute. In the first exposure, during warmup from −130°F, a thermal shock of 44°F/min occurred. In the second exposure, during warmup from −195°F, the panel experienced a thermal shock of 52°F/min. Electrical performance tests of the solar panel were conducted in sunlight before and after the thermal shock tests. Total panel performance remained above absolute minimum requirements. Some degradation of power output was measured, and physical examination of the solar panel prior to and following the thermal shock testing revealed some coverglass delamination.

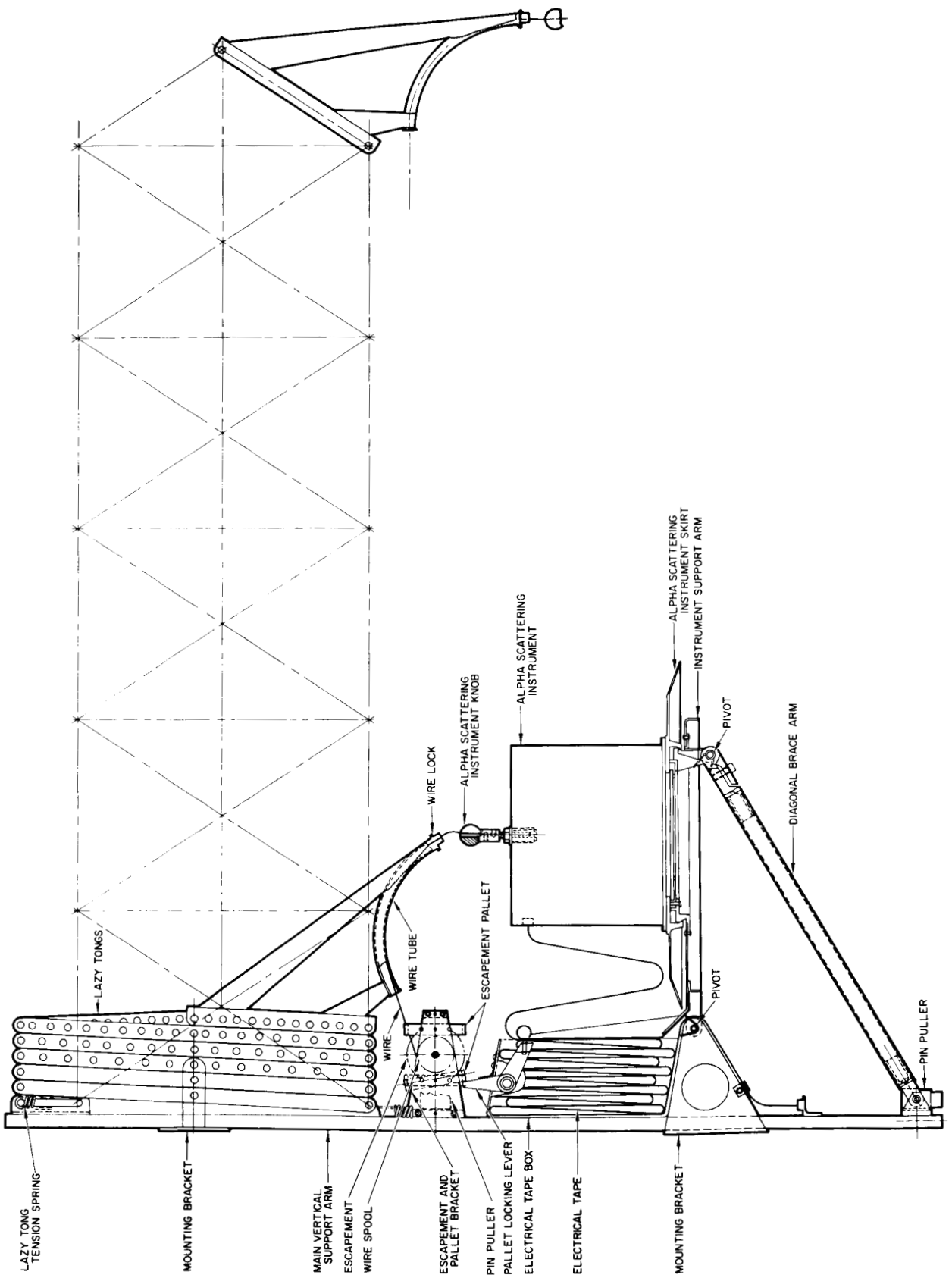

Fig. 2. Instrument sensor deployment mechanism for the alpha particle scattering experiment

F. Scientific Payload

1. Alpha Particle Scattering Experiment

The alpha particle scattering experiment will be used for compositional analysis of lunar surface materials. The experiment subsystem consists of an instrument, instrument auxiliary, instrument sensor deployment mechanism, mounting substructure, and associated cable harnesses. A sensor head assembly (deployed onto the lunar surface) and an electronics unit comprise the instrument.

Based on new deployment requirements and instructions to utilize a "lazy tongs" escapement mechanism, a redesign of the instrument sensor deployment mechanism has been initiated. In the new design (Fig. 2), the instrument support arm and diagonal brace arm (with an adjustable locking lever) provide an arrangement for clamping the skirt of the alpha particle scattering instrument to the supporting structure. An extension on the instrument support arm contains the electrical cable (accordion-folded) within an open box. This extension also bears against one end of the pallet locking lever, causing the other end to block movement of the pallet. This prevents the escape wheel and the spool on which structural wire is wound from rotating, thus keeping the wire taut. The other end of the wire goes through a Teflon-lined wire tube and then through a wire lock (clamped to the wire at the other end of the tube). The wire lock permits some slack between the tube and the instrument knob to which the end of the wire is attached. The tube is attached to the outer link of a spring-driven lazy-tongs device. A slotted nut rides on a threaded extension of the spool shaft, and a pinpuller rides in the slot.

Following touchdown, the alpha particle scattering instrument is deployed to a "background count" position away from the spacecraft and above the lunar surface. This is accomplished by an Earth command which actuates the pinpuller at the diagonal brace arm. When the pin is withdrawn, the diagonal brace arm drops away from the main vertical support, rotating the locking lever out of the instrument skirt and thus leaving it free. The instrument support arm also falls away, rotating about its pivot point near the main vertical support. When the instrument support arm falls away, it opens the door on the electrical harness storage box and releases the pallet lock, thus allowing the spool wire tension to operate the escapement.

The lazy tongs are driven to the extended position by helical and leaf springs. The escapement controls the rate at which the alpha particle scattering instrument moves to the background count position. At that point, the slotted nut reaches the end of the threaded portion of the shaft. Further rotation of the spool is prevented by the second pinpuller. An Earth command operates the second pinpuller, releasing the wire spool and allowing the escapement mechanism to unreel the wire at a maximum velocity of 0.7 ft/sec until the alpha particle scattering instrument is lowered to the lunar surface. After lunar surface operation, the soil mechanics surface sampler can be moved over the instrument knob, picking up the instrument and relocating it.

G. Propulsion

1. Vernier Propulsion Subsystem Evaluation

Work continued at JPL on the program to perform limited environmental tests of selected upstream system components for the purpose of evaluating, on an independent basis, the capability of these components to meet *Surveyor* requirements. The evaluation of a helium regulator's characteristics under temperature extremes was reported in *SPS* 37-32, Vol. VI, p. 10. The regulator testing has now been completed. The life cycle tests showed that, in the first of 20 cycles, the regulated pressure was above the upper limit at low flow rates and then remained within tolerance until the end of each series. However, the present regulator design (more recent than that of the model under test) incorporates a precalibrated spring package which gives a flatter regulator output. This enables the regulator to be calibrated so that the pressure will be within allowable limits. Also, the spring material has been changed in the modified design to correct problems of corrosion.

There were other areas found where improvements might be incorporated; however, the type-approval tests of both the old and new designs (not incorporating these possible changes) have not resulted in any failures in these areas. The improvements will be considered for future units.

The helium relief valve is the next component to be evaluated during this program. Two units have been acquired from HAC. One of these will undergo type-approval tests in its present configuration, and the other will undergo these tests with a modified seal design.

2. Thrust Chamber Assembly Evaluation

The evaluation of *Surveyor* vernier engines continued at the JPL Edwards Test Station. During this reporting period, a thrust chamber assembly filled with solvents was subjected to a three-axis simulated boost vibration test. There was no indication of leakage as a result of vibration, and solvent flow tests of the engine after the vibration test showed essentially no change in engine flow characteristics.

After being remounted on the shaker fixture, the engine was fired and subjected to simulated retromotor vibration pulses. The only anomaly that occurred was a shift in the mixture ratio during the second test, and the shift was within allowable limits. A similar shift was found on a thrust chamber assembly used in prequalification testing at the manufacturer's facility. Both were due to the inability of the self-locking adjustment screws to hold during severe vibration. The design was changed to incorporate a positive lock by epoxy seals. After the modified assembly completed type-approval and additional testing without evidence of failure, this change was incorporated into all thrust chamber assemblies.

When testing engine dynamics with saturated propellants, it was found that the presence of helium dissolved in the propellants had a significant effect on dynamic response, particularly at low thrust levels. A reduced-volume oxidizer line resulted in an improvement in response during step thrust changes. The test results also confirmed analytical predictions that a high propellant temperature would degrade dynamic performance.

Tests were then performed to demonstrate that start and shutdown characteristics, performance, and dynamic response would be unchanged in an acceleration field simulating the condition at retromotor burnout. The test data, when compared with previous firing data, indicated no detectable difference in operating characteristics.

3. Retrorocket Temperature Conditioning Tests

Temperature conditioning tests are being conducted with the thermal-control-model inert engine to simulate the ETR operations sequence. The tests completed thus far have established the retroengine assembly thermal time constant to be 50 hr. Therefore, the 72-hr minimum prelaunch conditioning period at 95 $\pm 3°$F would be sufficient to heat the retroengine from the 75°F nominal explosive-safe-area ambient temperature to the required launch temperature range of 85 $\pm 5°$F.

However, in the event of an abort requiring removal of the spacecraft to the explosive safe area for repairs, the planned 72-hr conditioning period could be reduced to as little as 14 hr. In this event, the retro would not be exposed to the 95 $\pm 3°$F conditioned environment for a sufficiently long period to guarantee the minimum launch temperature. It appears, therefore, that resistance heaters will be required on the retro case to provide a minimum launch temperature of 80°F under any conditions.

H. Test Facilities and Equipment

1. Guidance and Maneuver Analyzer

A model has been constructed to represent the *Surveyor* spacecraft and its associated flight geometry. This model (Fig. 3), known as the guidance and maneuver analyzer, is presently being used for development purposes and during premission tests and will eventually be used to analyze guidance and maneuver aspects during *Surveyor* missions. Although intended primarily for use in the *Surveyor* Project, the model has general application in the analysis of various phases of lunar and interplanetary missions.

2. Surveyor Spacecraft Test Facility

The *Surveyor* Spacecraft Test Facility (Fig. 4) is located approximately 7 miles from the Goldstone Pioneer Station. Natural site attenuation and adjustable attenuation simulate the realistic lunar distance for background or leakage radiation from the spacecraft. Activation of the facility began July 22 with the arrival of two 50- $\times$ 10-ft trailers to be used for maintenance, bonded stores, and office facilities. The power and communication lines were installed, and the refrigeration units were checked out. The system test equipment assembly trailer arrived July 27. Facility activation included the installation, checkout, and verification of the equipment necessary to perform the mission operations compatibility tests of the T-21 prototype system test spacecraft at the Goldstone Pioneer Station.

3. Command and Data-Handling Console Test Set

The command and data-handling console test set is composed of three drawers mounted in a half-rack roll-

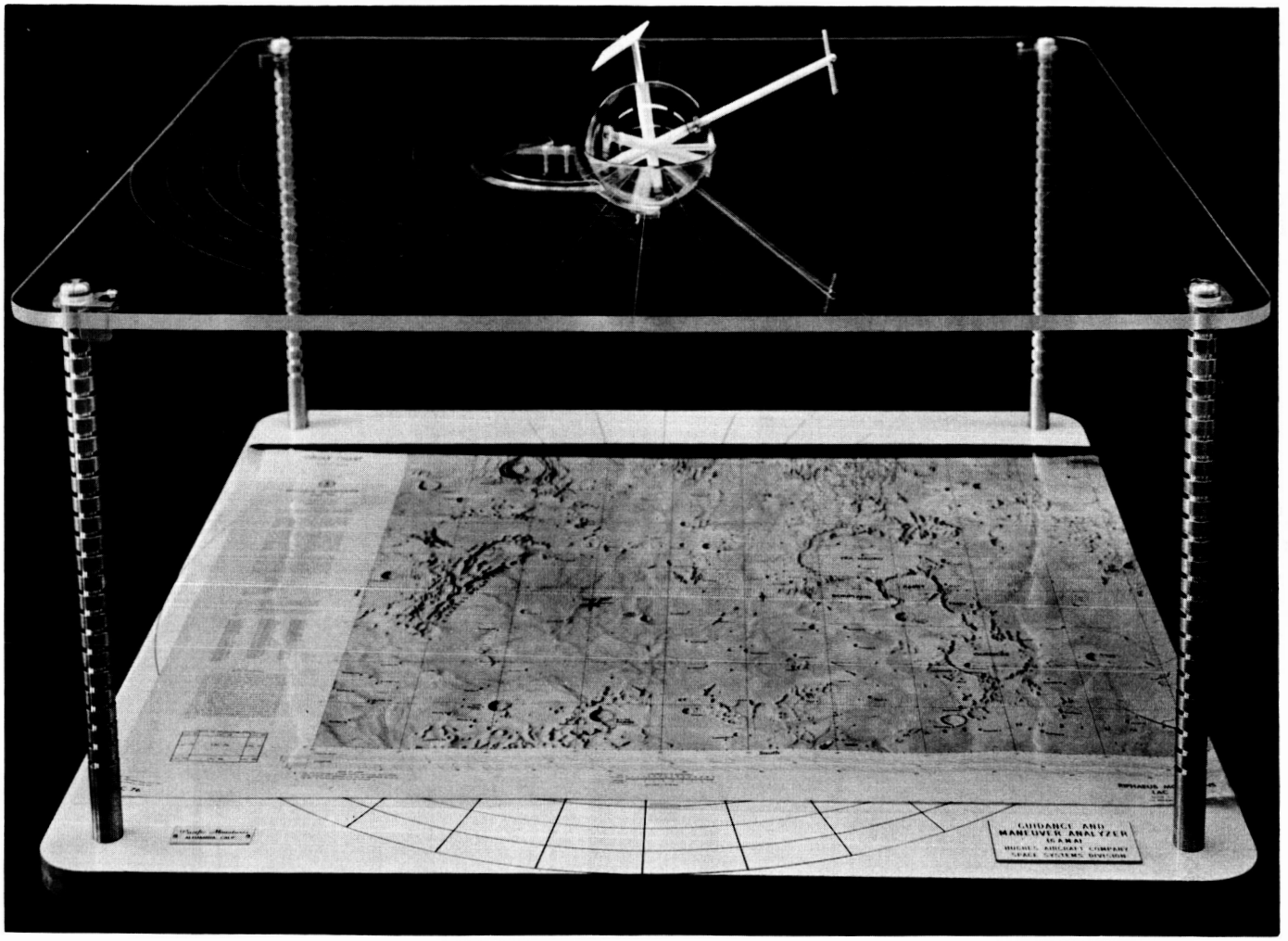

Fig. 3. Guidance and maneuver analyzer

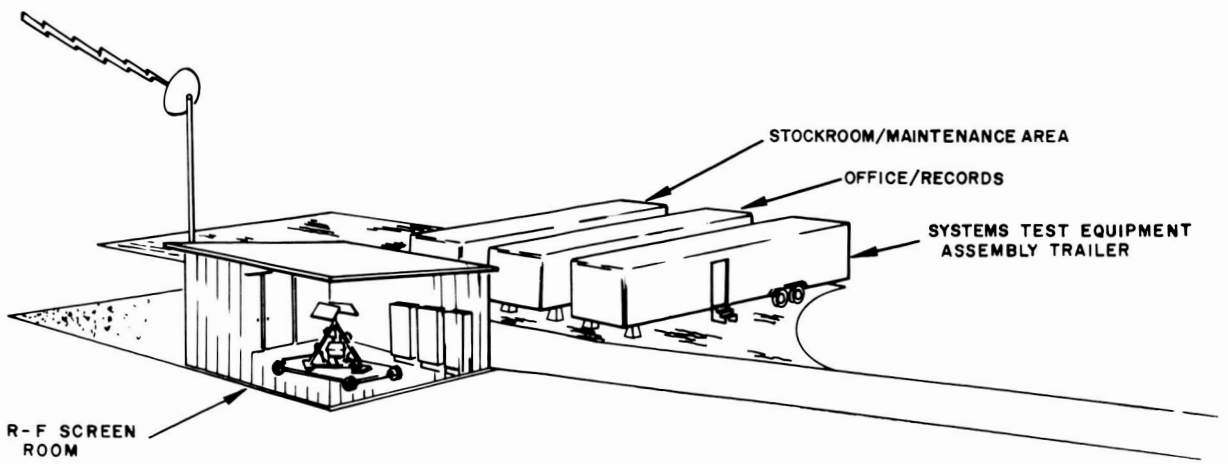

Fig. 4. *Surveyor* Spacecraft Test Facility

away cabinet: a signal drawer, a noise and output drawer, and a noise source drawer. The test set generates the necessary signals to test the console demodulator. Its 10-Mc output closely simulates the output of the RF system test equipment assembly receiver. Both the 10-Mc signal circuitry and the noise source contain step attenuators. The noise summing (noise and output) drawer contains a power meter. By use of this meter and the two step attenuators, a wide range of video or 10-Mc-output signal-to-noise ratios may be selected. Seven subcarrier oscillators contained in the signal drawer are used to modulate the 10-Mc output from the test set.

The command and data-handling console test set was calibrated and evaluated at System Test Equipment Assembly 4 during June. Checks were made with the console frequency-modulated demodulator to determine the signal-to-noise ratios that degraded the operation of the demodulator. The console's pulse-code-modulation simulator was used to modulate the test set's 70-kc subcarrier oscillator. Test results indicated that the test set will be a useful tool for testing and evaluating the command and data-handling console. After the completion of this testing, the test set was sent to the ETR to support test operations there.

PLANETARY–INTERPLANETARY PROGRAM

II. *Mariner* Project

A. Introduction

The early objective of the Planetary–Interplanetary Program was the initial probing of the planets Mars and Venus by unmanned spacecraft. The initial probing of Venus was successfully accomplished by the *Mariner II* spacecraft in 1962. The initial probing of Mars was successfully accomplished by the *Mariner IV* spacecraft during the 1964–1965 flight opportunity.

The primary objective of the *Mariner C* missions (*Mariner* Mars 1964 Project) was to conduct closeup flyby scientific observations of the planet Mars during the 1964–1965 flight opportunity and to transmit the results of these observations back to Earth. A secondary objective of the *Mariner C* missions was to provide experience and knowledge about the performance of the basic engineering equipment of an attitude-stabilized flyby spacecraft during a long-duration flight in space farther away from the Sun than the Earth. An additional objective was to perform certain field and particle measurements in interplanetary space during the trip in addition to those performed in the vicinity of Mars.

The *Mariner III* spacecraft was launched from the Eastern Test Range (ETR) on November 5, 1964. The nose cone failed to eject from the spacecraft, thereby precluding solar-panel deployment. The battery power was depleted 8 hr, 43 min after launch.

The *Mariner IV* spacecraft was successfully injected into a Mars encounter orbit about the Sun on November 28, 1964. The encounter with Mars, which occurred on July 14 and 15, 1965, was entirely successful. Flight operations were conducted as planned with a series of ground-transmitted commands: some to initiate spacecraft actions, with backup provided by automatic onboard features, and others to back up the critical automatic operations. Planetary observations were performed during the *Mariner IV* flyby which provided basic new information about Mars, including TV pictures, cosmic dust particle counts, and measurements of magnetic and ionizing radiation fields. The TV pictures were played back to Earth twice over a 20-day period without incident. In addition, an Earth occultation experiment was carried out during the Type I trajectory flyby to obtain data relating to the scale height and pressure in the

atmosphere of Mars. Analysis of the TV pictures and the data from the other science experiments is continuing. Preliminary analysis indicates the following characteristics of Mars:

(1) A very low (if any) magnetic field and, therefore, no measurable radiation field (by *Mariner IV* instruments).

(2) A Moon-like surface with many craters, and no evidence of atmospheric erosion or surface disturbance by volcanic action or crust upheaval.

(3) An atmospheric pressure in the 10- to 20-mbar region (10 mbar being the more likely value).

At the end of the second playback of the TV pictures, ground commands were sent to the spacecraft to once again return it to a cruise-mode condition. On August 30, the encounter sequence was rerun by ground command to take pictures of black space in order to provide a further calibration of the TV subsystem. Such a calibration should permit a better understanding of the received Mars pictures and will, therefore, enable a more knowledgeable enhancement of the pictures. A series of 11 commands was transmitted during this operation without incident, and the spacecraft performed perfectly.

The *Mariner IV* flight is continuing without significant changes in subsystem performance. The spacecraft is performing as designed and is being monitored continuously by the worldwide Deep Space Instrumentation Facility/JPL Space Flight Operations Facility network. It will be possible to receive telemetry from the spacecraft until about October 1, 1965, at which time the *Mariner IV*'s high-gain antenna pattern main lobe will no longer be pointed at Earth.

B. *Mariner IV* Space Flight Operations

The critical events which occurred during and after the *Mariner IV* encounter with Mars on July 14 and 15 are given in Table 1. Central computer and sequencer cyclic pulses were observed on schedule, one every 66⅔ hr, both before and after encounter. After encounter, the $+y$ solar vane moved in the adaptive mode with a one-data-number change. Disturbances in the roll channel of the attitude-control subsystem were noted on 4 days during July and on 1 day during August.

A TV calibration sequence was attempted on August 21 in hopes of performing an inflight calibration (black space) of the performance of the TV/recording subsystems in order to maximize the usefulness of the TV data obtained during planetary encounter. A secondary objective of the sequence was to take TV pictures of Altair, a first-magnitude star in the constellation Aquila, which was within the *Mariner IV* TV subsystem cone-angle field of view on August 21. However, it was necessary to cancel the sequence due to technical difficulties with the command transmitter.

C. *Mariner IV* Spacecraft Performance During the Mission

1. Structure

Mariner IV flight data indicated that the structure, electronic cabling, mechanical devices, and the electronic packaging performed as designed. Flight telemetry was obtained which verified the proper operation of various mechanical devices, including the separation-initiated timer and pyrotechnic arming switch, solar-panel deployment mechanisms, the cruise damper and latch, the scan actuator, the scan inhibit switch, and the science platform cover.

2. Thermal Control

Monitored temperatures remained within allowable limits throughout the flight. These temperatures were generally lower than prelaunch predictions, but other flight thermal performance was essentially as expected. The absorptivity standard provided valuable information regarding the degradation of thermal control surfaces in space, and a better understanding of the limitations of space simulator testing was thereby obtained.

3. Attitude-Control Subsystem

The *Mariner IV* attitude-control subsystem successfully performed all required functions from launch through the post-encounter phase of the flight. Anomalies were discovered in the star-sensor roll control system, the solar vanes, and the cold-gas thrusters. The only one

Table 1. Critical events during and after the *Mariner IV* encounter with Mars

Event	Date, 1965	GMT, hr:min:sec		
		Command transmitted	Command received	Event verified
Encounter science on command; start scan platform	July 14	14:27:55	14:40:32	14:52:31
Central computer and sequencer nominal command to start encounter sequence		—	15:41:49	15:53:49
Stop scan platform		17:10:18	17:22:55	17:34:55
Transfer to telemetry Data Mode 3 (all science data)		22:10:29	22:23:07	22:35:08
Planet acquired by wide-angle acquisition scan platform's wide-angle Mars sensor		—	23:42:00	23:54:42
Planet acquired by narrow-angle acquisition scan platform's narrow-angle Mars sensor; start video storage subsystem (or tape recorder)	July 15	—	—	00:29:22
Backup command for preceding event		00:11:57	00:24:36	00:36:37
Backup command for automatic spacecraft tape recorder turnoff		00:31:42	00:44:21	00:56:23
Six commands for turn-on of cruise science and telemetry Data Mode 2 (⅓ engineering data and ⅔ science data)		00:32:40 to 00:57:00	00:45:19 to 01:09:39	00:57:20 to 01:21:40
Spacecraft's closest approach to Mars		—	01:00:57	—
Spacecraft enters occultation and goes behind Mars; spacecraft's radio (RF) transmission signal to Earth blanked out by planet		—	02:19:11	02:31:12
Spacecraft leaves occultation; RF signal received on Earth		—	03:13:04	03:25:06
Central computer and sequencer command to turn off encounter science		—	05:01:49	05:13:52
Cruise science off; switch to telemetry Data Mode 4/1 (video storage subsystem recorded data/engineering data); initially Mode 1 only		—	11:41:50	11:53:53
Start of first playback of first TV picture by spacecraft's video storage subsystem; telemetry Data Mode 4		—	12:49:54	13:01:58
Completion of first playback[a] of TV pictures through the 22nd line of the 22nd picture; end telemetry Data Mode 4	July 24	—	—	19:26:33
Start of second playback of first TV picture by spacecraft's video storage subsystem; telemetry Data Mode 4	July 24	—	—	21:21:53
Completion of second playback of TV pictures through the 22nd line of the 22nd picture; end telemetry Data Mode 4	August 3	—	—	03:36:02
Return of spacecraft to cruise mode				
Command for turn-on of battery charger		03:08:33	—	03:36:02
Command for turn-off of planet science, cruise science, and battery charger		03:14:33	—	03:42:02
Command for switch to telemetry Data Mode 2 and turn-on of cruise science		03:20:33	—	03:48:02

[a]Playback sequence included 8 hr, 35 min of TV science data (Mode 4) and 1 hr, 57 min of engineering data (Mode 1) for each complete picture.

requiring corrective action was the star-sensor problem. Most evidence indicates that roll transients were caused by bright flashes, external to the spacecraft, which were detected by the star sensor. The use of a radio ground command to deactivate the brightness gate logic to prevent loss of acquisition was indicated and proved successful. The source of the continuing roll transients during the long cruise period is being investigated. One obvious solution to the roll transient problem is to provide logic circuitry to tie in the high brightness gate with the gyro shutdown signal. Whenever the gyros are off for cruise operation, the high gate would be removed; hence, a bright flash would not start a roll search.

During the encounter period, the only discernible attitude-control activity was the observable effect of the scan platform on the limit-cycle operation. This was expected and was used to verify proper scan operation. No planetary effects from Mars on the control system were observed, and no gravity gradient torques, atmospheric torques, stray light reflections, or radiation effects were detected.

4. Power Subsystem

During the cruise portion of the flight preceding encounter, power readings were constant, with a power demand from the solar panels of 164 w. Initiation of the encounter sequence increased the power demand to 197 w as expected. Stopping of the scan system platform was verified by the power subsystem when the main regulator output current decreased one data number.

At approximately 20:23 GMT on July 14 during the encounter sequence, the battery voltage decreased one data number due to increased battery temperature. This 3°F temperature increase resulted from increased power dissipation in the adjacent cases after turn-on of the encounter science.

Operation of the power subsystem was also normal after turn-on of cruise science and the switch to telemetry Data Mode 2. As expected, power levels exceeded those of normal cruise only by an amount equal to the 2.4-kc power to the tape recorder electronics. At 07:25 GMT on July 15, the battery voltage increased one data number, returning to its pre-encounter value. This increase was a normal result of the 1°F decrease in battery temperature that occurred at encounter science turn-off. Telemetry Data Mode 1 power data following the turn-off of cruise science were completely normal, with a power demand from the solar panels of 147 w.

After playback of the TV pictures was completed, the spacecraft was returned to cruise-mode operation. Power demand returned to its pre-encounter value of 164 w, and all power measurements were normal. At the end of the reporting period, the spacecraft was in a cruise mode, and all elements of the power subsystem were operating normally, with the possible exception of the battery with its higher-than-expected voltage (*SPS 37-33*, Vol. VI, p. 18; and *SPS 37-34*, Vol. VI, p. 20).

D. Future Operations for *Mariner IV*

When telemetry reception from the *Mariner IV* spacecraft ceases on approximately October 1, Phase 1 of the *Mariner* Project will be concluded. The Deep Space Network has determined that, if the spacecraft transmitter is returned to the omni- or low-gain antenna, it will be possible to track *Mariner IV* as an RF source completely around its orbit of the Sun. Invaluable celestial mechanics data for reducing the present uncertainty in the astronomical unit value and the ephemerides of the Earth and Mars could thus be provided. This surveillance period has been defined as Phase 2 of the *Mariner* Project.

During the latter half of 1967, the spacecraft will again be within telemetry reception range of the Earth. If the transmitter is still working at that time and if tracking schedules permit, it may be possible to recover additional cruise science information. This period has been defined as Phase 3 of the *Mariner* Project.

On August 26, a series of commands was sent to condition *Mariner IV* for Phase 2. A *midcourse maneuver inhibit* command was transmitted to ensure against an inadvertent maneuver which could occur if certain specific failures of the central computer and sequencer were to occur. Since positive confirmation that this command was effected is not possible, minimum pitch and roll turn commands and minimum motor burn commands were also sent to be stored in the central computer and sequencer registers. Normally, their post-maneuver state is for maximum turns and burn times.

On August 27, a *Canopus tracker cone angle update* command was transmitted to the spacecraft. This command was required to retain lock on the star Canopus for the remainder of Phase 1.

DEEP SPACE NETWORK

III. Deep Space Instrumentation Facility

A. Introduction

The Deep Space Instrumentation Facility (DSIF) utilizes large antennas, low-noise phase-lock receiving systems, and high-power transmitters located at stations positioned around the Earth to track, command, and receive data from deep space probes. The DSIF stations are:

Station	Location
Goldstone Pioneer	Goldstone, California
Goldstone Echo	Goldstone, California
Goldstone Venus (research and development)	Goldstone, California
Goldstone Mars (under construction)	Goldstone, California
Woomera	Island Lagoon, Australia
Tidbinbilla	Canberra, Australia
Johannesburg	Johannesburg, South Africa
Madrid	Madrid, Spain
Spacecraft Monitoring	Cape Kennedy, Florida
Spacecraft Guidance and Command (under construction)	Ascension Island

To improve the data rate and distance capability, a 210-ft-diameter Advanced Antenna System is under construction at the Goldstone Mars Station, and two additional antennas of this size are planned for installation at overseas stations. Overseas stations are generally operated by personnel of the respective countries.

It is the policy of the DSIF to continuously conduct research and development of new components and systems and to engineer them into the DSIF to maintain a state-of-the-art capability.

B. Tracking Stations Engineering and Operations

1. Goldstone Pioneer Station

Prior to the *Mariner IV* encounter with Mars, tests were conducted at the Goldstone Pioneer Station for training operations personnel and for determining command system capability at planetary distances. Practice command loop lockup tests with the spacecraft, using the 100-kw capability of the Goldstone Venus Station, were also performed. The results indicated that all systems were functioning well, with no apparent degradation of spacecraft response to commands due to distance.

The *Mariner IV* occultation experiment equipment, including a backup installation at the Goldstone Echo Station, was operationally tested. For backup support for the *Mariner IV* mission, a duplicate *read, write, verify* command console and a mission-dependent equipment console were installed.

The *Mariner IV* encounter with Mars on July 14 and 15, 1965, was recorded by the Goldstone Pioneer and Echo Stations, with the Goldstone Venus Station in a standby status to provide command transmission if needed. The TV picture-taking of the surface of Mars and the occultation experiment were both completed successfully, and, during the post-encounter period, the TV picture data were transmitted twice. The second recording of the pictures was completed by the Goldstone Echo Station, which then continued to track the spacecraft.

The Goldstone Pioneer Station preparations for the *Surveyor* Project have been progressing concurrently with the *Mariner IV* tracking operations. Most interface tests and a series of tests involving the use of *Surveyor* equipment located in the Microwave Test Facility screen room have been conducted. An enlarged screen room was constructed at the Microwave Test Facility, using parts of the former smaller room (*SPS 37-34*, Vol. III, p. 5). This room, 28 × 28 × 20 ft, is capable of housing the full-sized spacecraft. The installation of the *Surveyor* T-21 (prototype system-test) spacecraft (Fig. 1) enabled the start of the final *Surveyor* testing.

Through July, crew training tests were conducted on the ground equipment using tapes simulating the spacecraft action. In August, after the arrival of the T-21 spacecraft, crew training tests were started using the spacecraft located in the screen room. Simulated tracking, including transmission of commands and receipt of spacecraft telemetry, was conducted by microwave link. Tests were performed using the full system interfaces between the *Surveyor* ground equipment and the Pioneer Station S-band system. Received information

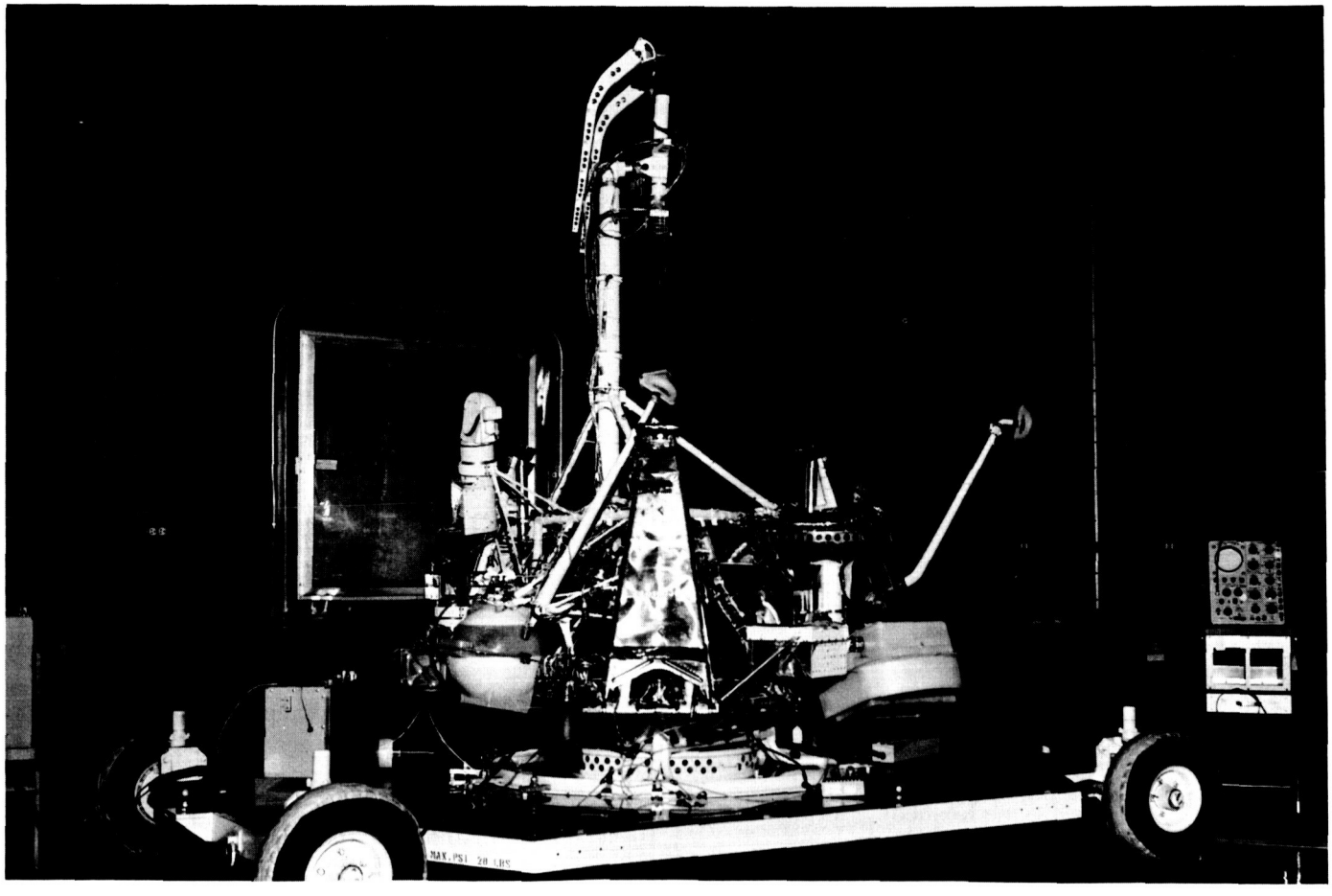

Fig. 1. *Surveyor* T-21 spacecraft in Microwave Test Facility screen room at the Goldstone Pioneer Station

was forwarded to the JPL Space Flight Operations Facility, simulating normal tracking operations. The tests covered simulated flight, landing, and postlanding operations. Spacecraft TV equipment was also tested. Testing is expected to continue until the time of the first mission.

2. Goldstone Echo Station

Installation of the S-band system at the Goldstone Echo Station began immediately after the completion of the *Ranger IX* tracking operations. Except for certain modified L-band modules and compatible test equipment and power supplies, the S-band system was essentially a completely new installation. Acquisition of the *Mariner IV* spacecraft for the first time on the night of June 15 (GMT) culminated the installation effort.

In late-June, the spacecraft was tracked in a series of tests to determine operational characteristics and to make all final adjustments to the S-band system. Beginning July 5, the Echo Station began daily tracking as backup to the Goldstone Pioneer Station from 30 min before the tracking transfer from the Johannesburg Tracking Station to the Goldstone Pioneer Station until 30 min after the Tidbinbilla Tracking Station had acquired. Two-way lock was not attempted due to the uncalibrated transmitter; if needed, the up-link lock could have been provided by the Goldstone Venus Station. However, by the week of the Mars flyby, the Echo Station was ready to provide full support to the Pioneer Station.

After the first TV data transmission from the spacecraft was concluded, the Echo Station stopped tracking to perform a series of peaking adjustments to the system in preparation for assuming full tracking responsibility as the prime station. Complete subsystem and system countdowns were performed daily, and the Echo Station was on a 15-min standby status for Pioneer Station support. Tracking resumed July 29, and prime station status was assumed by the Echo Station the following day.

A two-way lock with the spacecraft was established July 30. Until August 20, the Echo Station tracked intermittently in the two-way mode as a test of the system's capability to perform this function at planetary distances. Command loop lockup was accomplished on August 20 for the first time as a test of the 10-kw transmitter's capability to send commands to the spacecraft. Commands were sent on August 21. A variety of command experiments was performed, and, on August 26, commands were sent to inhibit the performance of a midcourse maneuver. The Canopus tracker cone angle was updated the following day. Commands to rerun the encounter sequence were transmitted August 30, and reception of the first TV picture began at the Echo Station at 02:06:01 GMT on August 31.

3. Goldstone Venus Station

The Goldstone Venus Station is continuing in the *Mariner* Mars 1964 transmit configuration and will remain as a command transmit station for the DSIF until October. During the Mars encounter, the Venus Station 100-kw transmitter provided the up-link signal which enabled the *Mariner IV* spacecraft to successfully establish the exit occultation spacecraft up-link lock. On August 2, the Venus Station transmitted the commands to the *Mariner IV* spacecraft which effectively turned off the transmission of the TV data and resumed the transmission of engineering and science data.

4. Goldstone Mars Station

Designated the Advanced Antenna System, a 210-ft-diameter antenna (Fig. 2) is under construction at the

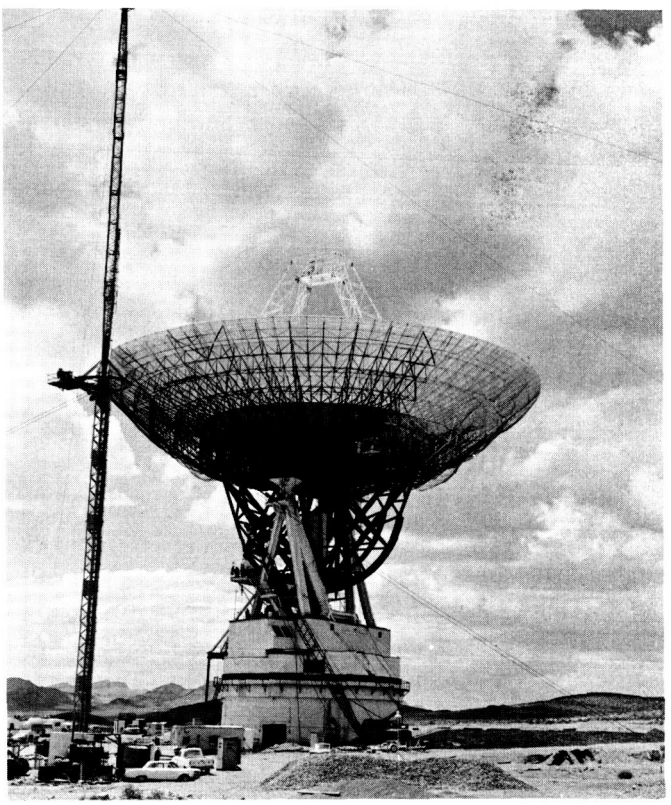

Fig. 2. Goldstone Mars Station 210-ft-diameter antenna

Goldstone Mars Station. The angular coverage of the antenna is ±300 deg in azimuth and +4 to 91 deg in elevation. The power distribution and air conditioning equipment, offices, and workshop areas are contained within the pedestal on the first floor. The antenna drive and S-band equipment control room are located on the second floor. Structurally isolated from the pedestal and the rotating alidade is the central instrument tower, on top of which is the precision angle data (master equatorial) equipment for pointing and steering the antenna. Located within the outer wall of this tower and enclosed in a central circular room, the cable wrapup provides for all power, signal, air conditioning, and hydraulic cables and permits rotation of the antenna about the azimuth axis.

The Advanced Antenna System at the Mars Station is nearing completion. All major structural components have been erected, and azimuth and elevation rotation under servo power has been accomplished. Initial elevation rotation was made August 6, when the reflector structure was rotated from the zenith to the 20-deg-above-horizon position. Adjustment of the gears and drives is in progress. Installation of electronic components is scheduled to begin in late-December.

5. Woomera Tracking Station

The Woomera Tracking Station S-band test installation is receiving a continuing operational performance evaluation at the Goldstone Pioneer Station. Personnel from Australia who made the present installation and who will also make the installation at Woomera are receiving training in its operation and maintenance. All necessary documentation and procedures are being prepared to accompany the transfer of the system to Woomera. During the week preceding and including the *Mariner IV* encounter with Mars, the Woomera personnel assisted in tracking operations at the Goldstone Pioneer and Echo Stations.

6. Johannesburg Tracking Station

A modified "suitcase" telemetry receiving system (*SPS 37-31*, Vol. III, p. 8) was integrated with the L- and S-band tracking system at the Johannesburg Tracking Station to provide wide-band telemetry capability for the first *Surveyor* mission. As shown in Fig. 3, the suitcase receiver was connected by a directional coupler to the existing 85-ft-diameter antenna and traveling wave maser in parallel with the existing L- and S-band receiver. To compensate for line loss, a tunnel diode amplifier was positioned in the suitcase receiver channel.

To provide the necessary telemetry outputs and levels, the suitcase receiver was modified using the following Goldstone duplicate standard S-band receiver components: a four-channel band-pass filter, a phase shifter, a 10-Mc intermediate-frequency amplifier, a video amplifier, and two variable attenuators. Since the receiver is to remain in use for an extended period at the Johannesburg Tracking Station, the battery power supplies were replaced with a commercial electronic power supply, and components mounted in a rack were added. With these added components, the receiver has three standard bandwidths: 4.5, 20, and 420 kc. It also has a predetected 10-Mc output for frequency-modulated telemetry of gyro speed data. In its present configuration, the receiver is not intended for TV reception.

When a complete Goldstone duplicate standard S-band receiver is installed at the Johannesburg Tracking Station, the suitcase telemetry receiver will be restored to its original condition as a portable receiver.

7. Spacecraft Guidance and Command Tracking Station

Assembly and testing of the Spacecraft Guidance and Command Tracking Station S-band system is in progress at the Goldstone Pioneer Station (*SPS 37-34*, Vol. III, p. 4). Personnel who will make the installation on Ascension Island are receiving instruction on the receiver, the analog instrumentation, the microwave equipment, and the ranging subsystem. Subsystems are being operationally tested as they arrive, and interface tests are being conducted as the system assembly continues.

A mockup (Fig. 4) of the 30-ft-diameter azimuth–elevation antenna for the Ascension Island station has been erected at the Pioneer Station for purposes of mechanical design development and initial component integration of the antenna microwave subsystem on the antenna structure and within the antenna-mounted electronics room. The mockup also serves as an aid in the design and development of the cable wrapup mechanism.

The primary antenna mechanical structure has been shipped to Ascension Island for erection and installation. The equipment remaining at the Pioneer Station is scheduled for disassembly, packaging, and shipment to the Spacecraft Guidance and Command Tracking Station in September. Following completion of the installation and system integration there, system tests of the complete station are scheduled to begin in early-1966.

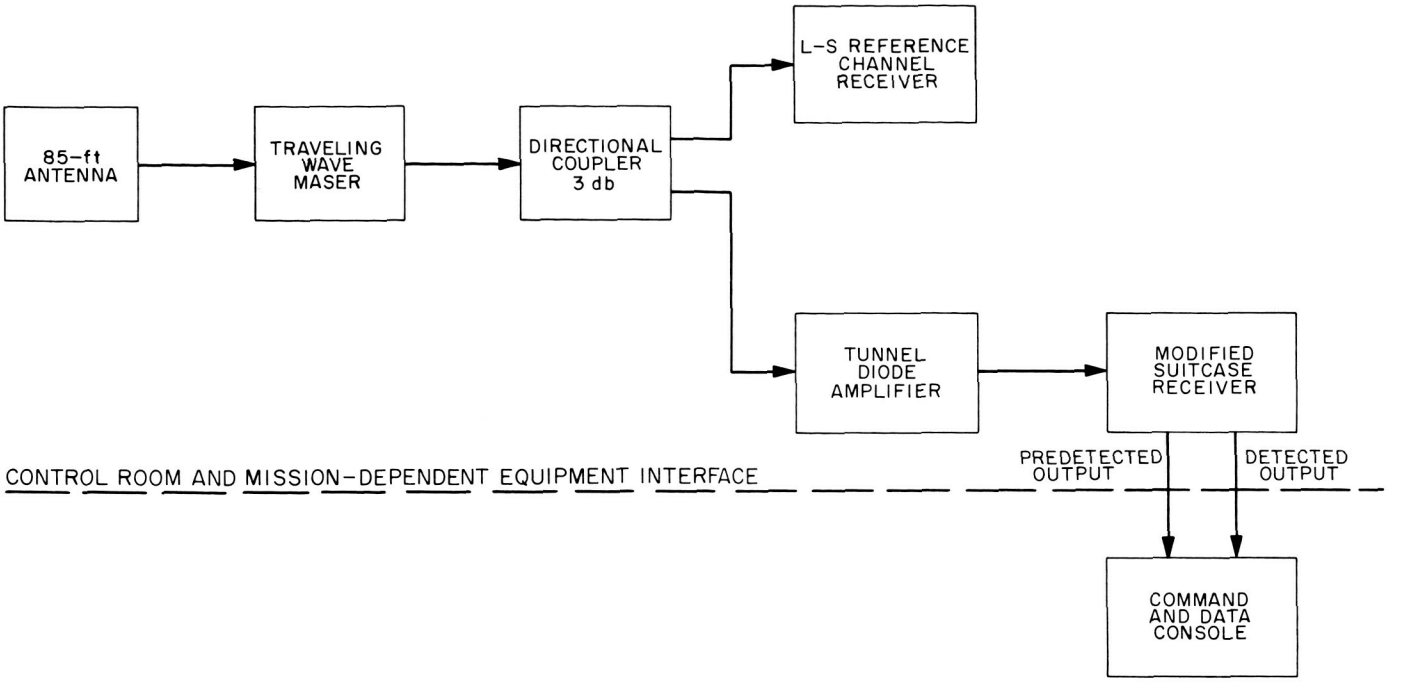

Fig. 3. L- and S-band receiver and integrated suitcase telemetry receiver

Fig. 4. Pioneer Station mockup of 30-ft-diameter azimuth–elevation antenna for the Spacecraft Guidance and Command Tracking Station

C. Developmental and Testing Activities

1. Amplitude-Stabilized Signal Source

A signal-amplitude-leveling system is being developed for use during antenna gain and pattern measurements. Operating in conjunction with a signal generator and a traveling wave tube, the system is expected to reduce: (1) the difficulty in making gain and pattern measurements, and (2) power drifts which lead to measurement errors. The design goal is an amplitude stability of ± 0.05 db.

One technique used for measuring antenna gain is the direct measurement of the power input to the collimation tower antenna and the power output at the terminals of the receiving antenna. The stable source is being developed because power drifts sometimes occur rapidly and thus cause difficulty in the simultaneous determination of radiated and received power. The system will level the signal at the input of the collimation tower standard gain dish.

The amplitude-stabilized signal source is shown in Fig. 5. The signal fed into the radiating dish is sampled by means of a directional coupler, and the coupled portion is converted into DC by a crystal video detector. The detector output is then proportional to the radiated power. A summing junction is used to compare the detector output and a DC reference voltage, and any resulting error voltage is integrated and used to drive the voltage-controlled attenuator, which then makes corrections for the error.

Testing showed that temperature control of the integrator, detector, and directional coupler is necessary. Final testing has not been completed, but temperature stability of the order of degrees should be adequate. No further tests are planned until final packaging (now in progress) is completed. However, the system has operated with no temperature control for a 17-hr period in a laboratory environment, and the total drift, including that at the power meter, was < 0.03 db.

2. Test Signal Control Assembly

The complexity of the DSIF tracking and communications system necessitates integrated, accurate, reliable, and convenient calibration and fault-finding instrumentation (*SPS 37-28*, Vol. III, pp. 29–39). To instrument such a program, a number of provisions were designed into the basic RF circuitry to allow monitoring or injection of microwave test signals by means of a test signal control assembly. The assembly is composed of a test signal control panel mounted in the parametric amplifier control rack, a test signal control box mounted on the support structure of the high-gain antenna, and associated control cables. The switching capabilities provide for remote selection of any of several microwave test signals and for application of the test signal to any of various test points within the receiver system. During a station countdown, the test signal control assembly becomes the control center for the reference RF and exciter signals. Calibration of the subsystems from the maser or parametric amplifier to the recording equipment is obtained by applying reference signals controlled by the assembly.

3. Traveling Wave Maser Performance During the Mariner IV Mission

Successful operation of all traveling wave masers was achieved during the *Mariner IV* encounter with Mars. A weekly reporting to JPL from the daily log of the pertinent pressures and temperatures in the closed-cycle refrigerator was required to optimize reliability and performance. During the encounter period, the reports were received daily, and, whenever necessary, telephone conferences were established with the various station operators. Graphs of the important data, which were plotted for each station on a continuing basis, proved to be very effective in diagnosing troubles and warning of impending failures. In addition to indicating routine

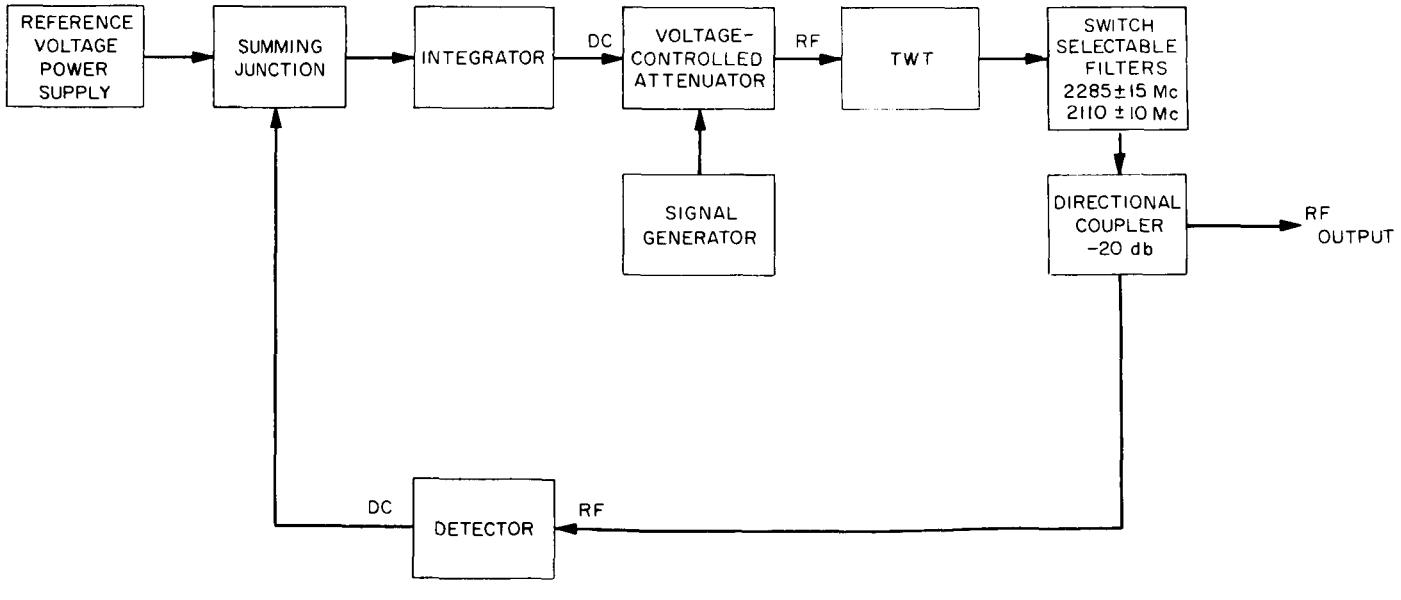

Fig. 5. Amplitude-stabilized signal source

troubles, these graphs were used to discern more subtle difficulties. There have been no known failures in the electronic equipment associated with the maser subsystem.

4. Goldstone Computer Facility

The Goldstone Computer Facility is a digital data processing center located at the Goldstone Space Communications Station. The basic functions of the facility (*SPS 37-30*, Vol. III, p. 17) are the reduction and analysis of tracking data, the making of pre- and post-flight calibrations, and the conducting of performance studies on improved tracking data monitoring techniques. In order to handle the growing work load in these areas, the Scientific Data System (SDS) 920 digital computer was recently replaced with a more advanced SDS 930 computer.

The SDS 930 computer is a high-speed general-purpose digital computer. The main frame consists of five racks which contain 8192 24-bit words of core storage, 16 priority interrupts, power supplies, and time-multiplexed communication channels. The memory cycle time is 1.75 μsec. Fig. 6 shows the basic SDS 930 computer with some of its peripheral equipment, which includes a 60-character/sec paper tape punch, a 300-character/sec paper tape reader, and a 10-character/sec teleprinter. These devices, which are common to most medium-sized computer systems, provide a means for loading and controlling the operating programs. Additional peripheral equipment provided on this computer system for bulk input and output are four magnetic tape transports, a line printer, and an IBM card reader–punch. Two channels for special input–output are provided, allowing direct input of teletype information and direct output of plotter data to a Benson–Lehner point plotter.

5. Spacecraft Visibility Program

A computer program, called the Spacecraft Visibility Program, to calculate and plot the range of visibility of DSIF antennas has been developed at JPL. The program is written in FORTRAN II language for the SDS 930 computer at the Goldstone Space Communications Station. Input is by punched card, digital output is on a line printer, and visual output is on an electroplotter which has been converted for on-line usage. When the location of the antenna (longitude and latitude), type of antenna, horizon mask, antenna limits, and spacecraft altitude are known, a plot made on a Mercator map of the world will show how far away the spacecraft

Fig. 6. SDS 930 computer and peripheral equipment

can be seen. The program is capable of calculating for any existing or theoretical antenna and location.

In the DSIF, there are two types of antennas utilizing two different coordinate systems: azimuth–elevation (az–el) and hour angle–declination (HA-dec). The 85-ft Goldstone Echo and Pioneer Station antennas are HA–dec, and the 85-ft Goldstone Venus Station antenna and the new 210-ft Goldstone Mars Station antenna are az–el. The HA–dec coordinates have the advantage of being easily converted to Earth coordinates, greatly simplifying relationships between coordinates of stations at different locations, but have the disadvantage of imposing structural limitations on the visibility of the antenna.

The horizon mask is the configuration of the local horizon which blocks the view of the antenna. There are usually gaps in the horizon mask data. To fill these gaps or to work for an antenna where the mask is unknown or nonexistent, the program can generate its own theoretical horizon.

The antenna limits are mechanical restrictions on the antenna. In HA–dec antennas, there is a major HA and a major dec limit. The HA limit is most often at 90 and 270 deg.

A minimum of four cards is input: (1) one card containing the number, longitude, and latitude of the station; (2) another card containing three indicators telling (a) whether the antenna is az–el or HA–dec, (b) whether a horizon mask will be given or whether the program should generate a theoretical horizon, and (c) whether the antenna has the usual HA limit or whether the HA limit will be input; (3) the third card giving the spacecraft altitude; and (4) the last card showing the dec limit. If a horizon mask is indicated as input, then a deck of the mask data follows the dec limit card. If the HA limit is to be input, a card containing the limit precedes the dec limit card. From this information, the program calculates local x,y,z coordinates, transforms these to an Earth-centered x,y,z system, and then calculates the longitude and latitude of the viewed spacecraft. The longitude and latitude are projected onto a Mercator world map of any scale and plotted. The result is easily converted to a reproducible form, eliminating long and tedious manual conversion of the data.

Plans for the program include producing separate overlays for each existing DSIF station. These, when placed over readily available Mercator world maps and gathered for the stations used in a particular mission, will enable a picture of total visibility in a minimum amount of time. The flexibility of the program will allow visibility plots to be drawn to aid in the evaluation of proposed antenna configurations and locations. Used with an existing program that plots satellite paths on a Mercator map, the program will enable quick indications of when a particular satellite will be in and out of view. Also, a simple internal change of one constant would allow the program to produce visibility plots for antenna sites such as a tracking station on the Moon.

IV. Space Flight Operations Facility

A. Introduction

The Space Flight Operations (SFO) Facility, located in a three-story building at JPL, utilizes operations control consoles, status and operations displays, computers, data-processing equipment for analysis of spacecraft performance and space science experiments, and communication facilities to control SFO. This control is accomplished by generating trajectories and orbits and command and control data from tracking and telemetry data received from the Deep Space Instrumentation Facility (DSIF) in near-real time. The SFO Facility also reduces the telemetry, tracking, command, and station performance data recorded by the DSIF into engineering and scientific information for analysis and use by the scientific experimenters and spacecraft engineers.

B. Simulation Data Conversion Center

The Simulation Data Conversion Center of the SFO Facility was developed to satisfy continuing Deep Space Network requirements for a means of realistically exercising the data handling elements of the SFO Complex in support of lunar and planetary projects. The center is designed to exercise and verify individual and combined operations of computer programs, hardware subsystems, and operational analysis teams. Present capabilities include the pretest preparation of simulated spacecraft tracking and telemetry data, the playback of data during tests, and the coordination of test activities to enhance realism and ensure adherence to the test plan.

1. Phase I

The development of the center is proceeding in phases, with Phase I having been completed in August 1965. The Phase I Simulation Data Conversion Center is located on the second floor of the SFO Facility and consists of a small general-purpose digital computer, the Programmed Data Processor 1, having special input–output capabilities; three FR 600 analog tape transports with record and playback electronics; a voice communications system interconnected to that of the SFO Facility; and facilities for preparation, reception, and transmission of data by teletype. Also, special communication lines

are provided to permit the insertion of data at points within the SFO Facility.

The Phase I center has been used extensively in preparation for the early *Surveyor* missions. Experience gained in this use is currently being applied toward the development of the Phase II center with a more advanced capability.

2. Phase II

The Phase II Simulation Data Conversion Center is being designed to permit a more realistic real-time response during mission tests than is presently available. A two-mission simulation capability is also being incorporated. This will not only permit the concurrent control of two simultaneous mission tests, but will also provide for testing of new simulation programs and the generation of data packages for remote station use.

To expedite the real-time response capability, the Phase II center will be organized into: (1) an operations area containing the data handling hardware and operators, and (2) control areas from which the operation of mission tests may be controlled. Consoles will be included in each control area for monitoring and talking on the SFO Facility operational voice communications system and the closed-circuit TV system and for monitoring and controlling operations of the center's operations area.

Functionally, the center will be divided into three subsystems which simulate activities within an SFO: a spacecraft simulator, a DSIF simulator, and a NASCOM simulator. The spacecraft simulator, which will simulate data normally telemetered by a spacecraft during a mission, will be composed of telemetry data profile, spacecraft commutator, signal generator, and command perturbation systems. The DSIF simulator will simulate the functions performed by the DSIF stations during a mission that are reflected within the SFO Facility operation. Receiver, telemetry data recovery, on-site data processing, telemetry data recording, trajectory data profile, tracking data handling, transmitter, and administrative data generation systems will be included. Circuit routing and communications perturbation systems will be included in the NASCOM simulator in order to simulate the functions performed by the worldwide NASCOM communications network during an SFO.

The Phase II Simulation Data Conversion Center is scheduled to be operational in late-1966 and will serve as an integral part of the over-all Deep Space Network mission simulation system.

C. *Mariner* Master Data Library

Since August 1964, a program has been under way for the design, development, and implementation of a master library of all data received and recorded during the *Mariner* Mars 1964 missions. This master data library will be the best source of telemetry and tracking data received and recorded by the DSIF during the *Mariner IV* mission, as well as discrete DSIF instrumentation performance parameters. The primary purpose is to produce a history of the *Mariner IV* mission from which postflight analysis of the spacecraft subsystems, scientific payload, and trajectory and the DSIF performance may be accomplished.

To afford a flexible and expedient access to data in the master data library, the system is categorized into three data groups: telemetry, tracking, and comment. The telemetry data are a series of the following two types of digital recorded magnetic tapes generated by the IBM 7094 computer programs: (1) station master merge tapes, containing the best telemetry data (derived from the demodulator input and output and the teletype encoder output) and ground instrumentation performance parameters recorded at each DSIF station during a *Mariner IV* pass; and (2) composite master merge tapes, containing a continuous sequential stream of the best telemetry data received from the composite of DSIF stations receiving and recording telemetry data (station master merge tapes) during each day of the *Mariner IV* mission. The tracking data are derived from both real- and non-real-time data, both of which are maintained on digital recorded magnetic tapes in formats compatible with the tracking data processor program and the orbit data generator program (which are, in themselves, user programs). Raw tracking data recorded on teletype paper tapes are maintained as part of the library. To explain peculiarities and/or anomalies occurring in both the telemetry and tracking data tables, the supporting SFO logs and master data library processing logs are maintained in the comment data table, which is recorded on microfilm.

SUPPORTING ACTIVITIES

V. Environmental Test Facilities

A. Six-Channel Automatic Accelerometer Selector

Vibration exciter systems utilize feedback control to maintain the desired acceleration imparted to the item under test. An accelerometer mounted on the test item produces a voltage proportional to the acceleration at that point. This voltage is fed back to the vibration exciter system electronic servo input in order to control the test.

Vibration testing of large structures such as spacecraft requires special attention to acceleration control. When vibration testing such structures, it is desirable to use more than one accelerometer as a control reference because the inherent non-rigid characteristics of large structures result in acceleration gradients. A single accelerometer can measure only one point and cannot provide a reference signal representing the entire structure under test.

A control system has been developed at JPL that maintains a constant acceleration level by selecting the peak signal from six accelerometers strategically located about the test item. This system is used in conjunction with a B & K Instruments, Inc., electronic servo for sine-wave testing and an automatic spectrum equalizer for servo control of random vibration testing. It is the last function that makes this system unique. The automatic spectrum equalizer requires frequency information for servo control during random noise vibration testing. Until the development of this selector, it was necessary to control random noise vibration testing using a single accelerometer or multiple accelerometers utilizing averaging techniques which could not provide frequency information. The accelerometer signals were monitored on an rms meter, and the gain of the system was adjusted manually.

Fig. 1 is a block diagram of the six-channel automatic accelerometer selector, and Fig. 2 shows two views of the completed prototype. The heart of this control system is the logic circuit that continually monitors the six accelerometers and selects the highest output for the feedback control signal. The six accelerometers are coupled directly to six input amplifiers. The AC signals are amplified and then rectified to produce a DC voltage proportional to the accelerometer input signals. These DC signals are

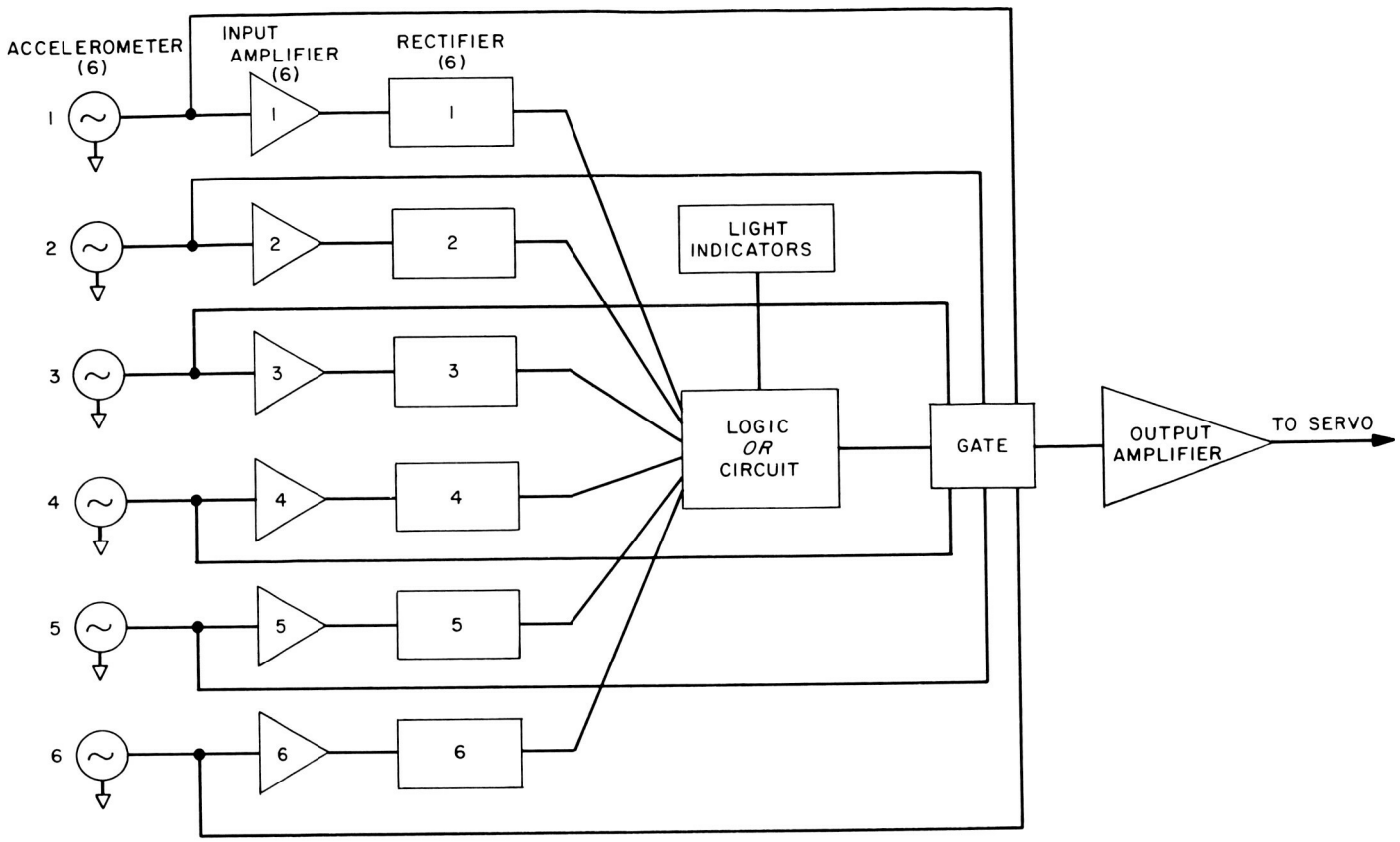

Fig. 1. Six-channel automatic accelerometer selector

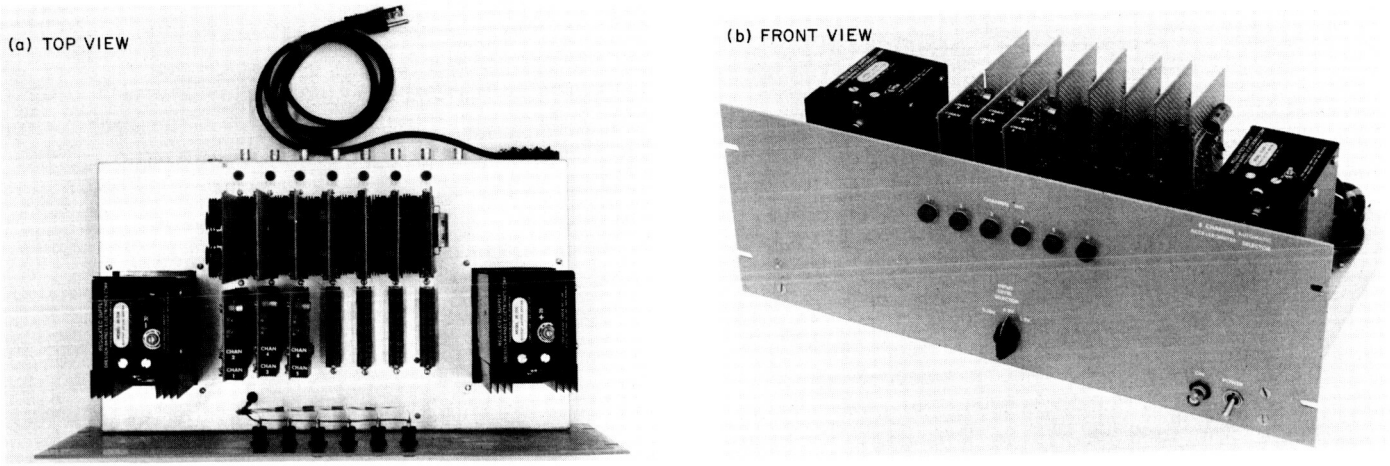

Fig. 2. Selector prototype

coupled to a logic *or* circuit which controls the gates. Only the peak signal that has the highest DC value at any instant of time is gated through to the output amplifier. The output amplifier provides isolation between the selector and servo circuits, as well as gain which is adjustable from 1 to 10. It is the output amplifier signal that determines the error voltage sent to the servo control system.

The advantages of this system are as follows:

(1) Control redundancy. If during a test one accelerometer fails, the remaining five accelerometers will provide the reference test level, thus assuring no overtesting, except perhaps at the point of the lost accelerometer.

(2) Spatial averaging. Six accelerometers mounted on a test fixture will reduce any acceleration gradient

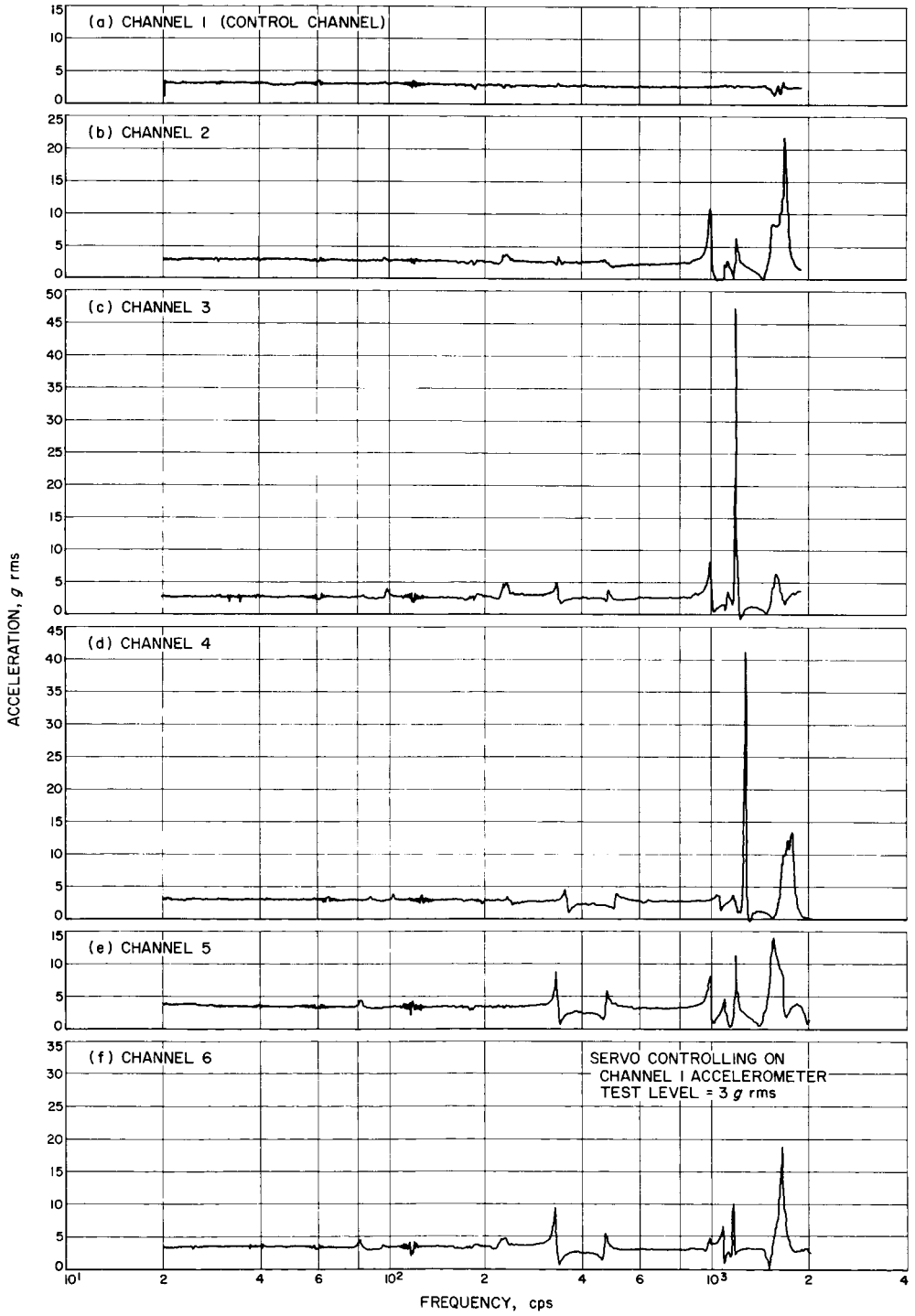

Fig. 3. Acceleration data utilizing single-channel control

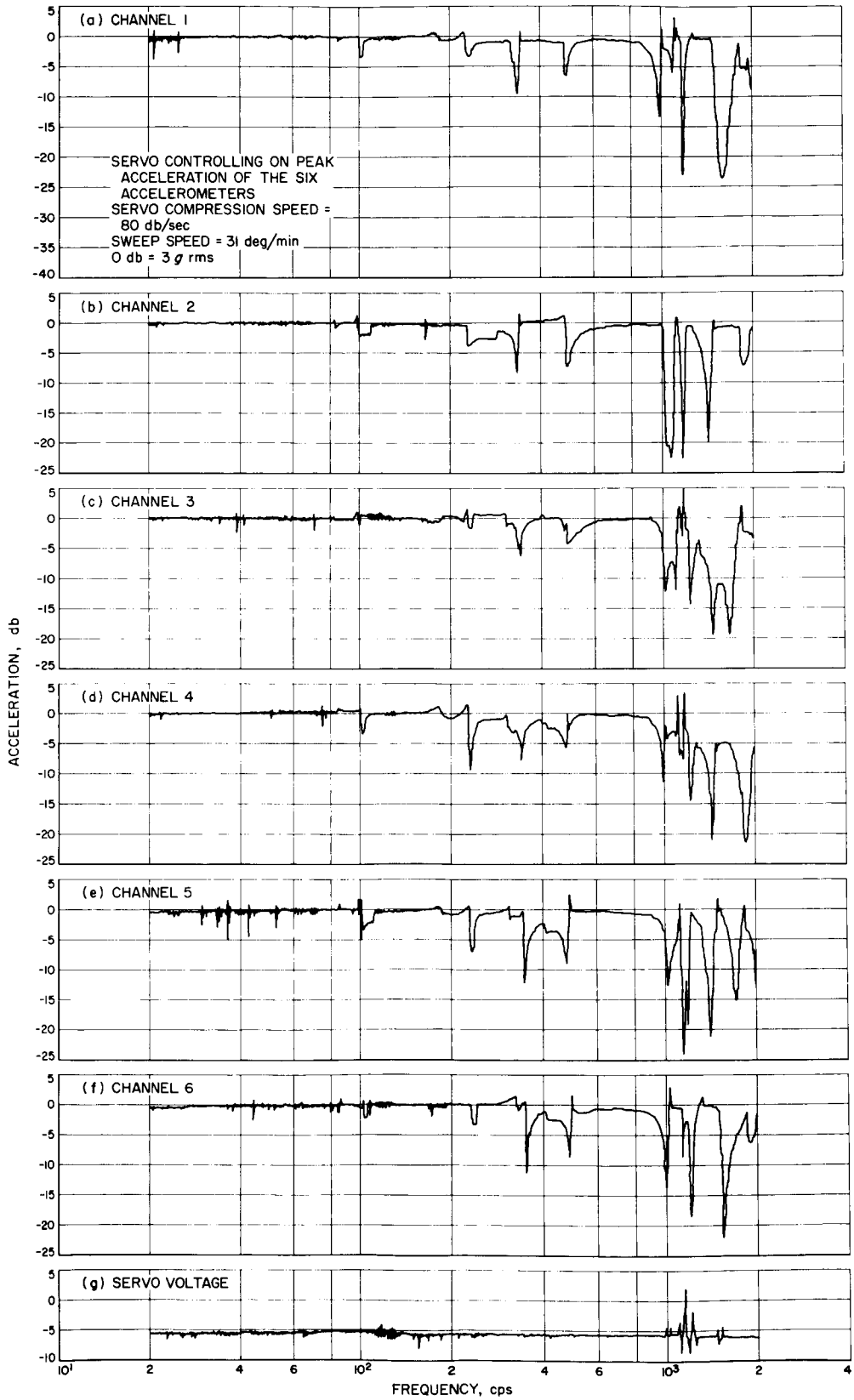

Fig. 4. Acceleration data utilizing six-channel automatic control

occurring on the test fixture since the fixture and test specimen act as a transmission line; i.e., parts of the structure are in an acceleration null while other parts are being subjected to peak acceleration.

(3) Time averaging. Over a given period of time, the average peak signal of six accelerometers will provide a more realistic acceleration level than that of one or two accelerometers. This concept is equivalent to plotting more points on a graph in order to obtain a smoother curve.

(4) Reduction of accelerometer calibration error. Any error resulting from improper calibration of a particular accelerometer will tend to be reduced in magnitude by using the selector.

The plots in Fig. 3 were obtained using a test setup wherein the vibration level was controlled by only one of six accelerometers, Channel 1 being the control accelerometer. Note that the other five accelerometers monitored levels as high as 40 *g* rms, even though Channel 1 was kept at the required test level of 3 *g* rms.

Fig. 4 illustrates the six-channel control system capability. The vibration level was controlled by all six accelerometers, and the required level was kept at 3 *g* rms over most of the frequency range. Channels 3 and 4 experienced extreme acceleration peaks at about 1400 cps. Although the servo lost control at this point, the test level never exceeded 5 db[1] of the desired level.

If more than six channels are required, two or more selectors can be connected in such a manner that the output from one selector is fed into one of the six channels of the next selector. The output amplifiers would be set for unity gain.

This control system concept is particularly useful for multiple vibration exciter systems. The net response at each point on a load attached to a multiple vibration exciter system is affected by the modal coupling from each shaker to that point. Thus, from point to point and from one frequency to another, the response varies widely. The only way to provide an effective feedback signal is to choose several points on the specimen and to control the test using diversity techniques, such as the largest of the signals or the signal average.[2]

In conclusion, whether employed with single or multiple vibration exciter systems, this control method establishes a more representative acceleration reference. The possibility of subjecting the item under test to higher levels of acceleration than those specified is thus minimized.

---

[1] 0 db = 3 *g* rms.

[2] Ratz, Alfred G., *Multi-Force Vibration Systems—The Next Generation,* Second Environmental Engineering Symposium, London, England, May 20, 1965.

SPACE SCIENCES

VI. Space Instruments

A. Preparations for the Analysis of *Surveyor* Video Data

1. Introduction

The *Surveyor* Space Science Analysis and Command (SSAC) Group in the JPL space flight operations organization is responsible for: (1) the organization and conduct of that portion of a *Surveyor* mission related to the operation of the scientific instruments on the payload, and (2) the evaluation of the data obtained. For the first mission, the instrument payload consists of a survey TV camera. The Television Performance Analysis and Command (TelPAC) Group, part of the SSAC organization, is composed of technical specialists who analyze and evaluate instrument performance and control the engineering performance of the TV experiment.

2. Responsibilities of the Video Analyst

As one of the technical specialists in the TelPAC Group, the video analyst's primary task is to monitor the video data displays, analyze the data, and determine the electronic performance of the TV instrument. After a successful lunar landing and prior to opening of the mirror on the TV instrument, an analysis of the video data will reveal the amount of noise in the video signal and the dark signal level or black reference. During a picture-taking sequence with the TV mirror stepped open, the video analyst will determine:

(1) Nominal signal-to-noise level at any specific time.

(2) Video signal amplitude as a percentage of full saturation level.

(3) Sharpness of focus (electronic and optical).

(4) Video content and contrast in the data.

The video analyst must also be prepared to detect malfunctions or anomalies with the instrument operation, analyze the cause, and recommend corrective action. Examples of such anomalies are: (1) dark picture—underexposed, (2) saturated picture—overexposed, (3) out-of-focus picture, (4) shaded picture, and (5) video data that are inconsistent with TV identification data or commands transmitted to the spacecraft.

3. Equipment

A video data display presently consists of a slow-scan TV monitor and a Type 564 storage oscilloscope (Fig. 1). This equipment will eventually be part of an engineering console to be used by the TelPAC Group. The slow-scan monitor is capable of operating at either the *Surveyor* TV normal-mode 1.2-sec frame time or the 20-sec emergency-mode frame time.

During a mission, it will be necessary to obtain photographs of the video data displayed by the slow-scan monitor and the oscilloscope. Difficulties have been experienced during training exercises in monitoring the video data and photographing them using the one set of display equipment. It is planned to obtain another slow-scan monitor and oscilloscope with polaroid oscilloscope cameras in order to obtain the required photographs.

4. Training Exercises

During training exercises, a prototype *Surveyor* TV camera known as the 4.2.2 camera is used as the source of video. The video data are displayed on the monitoring equipment simulating the operations of a real mission. The A-trace display on the oscilloscope, which allows the video signal to be seen in analog form, is valuable in determining signal-to-noise ratio, video amplitude, black- and white-level amplitudes, and sharpness of focus. The monitor display exhibits picture content and contrast.

The 4.2.2 camera has been used in three different configurations for the training exercises:

(1) The camera is positioned and focused on a screen, where an image is projected by a 35-mm slide projector using the rear projection technique. The azimuth and elevation positions of the camera mirror are not physically changed, but appear to change from an analysis of the video data. The realism of the data is due to the projection of different images or scenery. The iris and filter wheel are physically changed at various times to adjust for image intensities.

(2) The camera is installed inside a large circular area called the panorama (Figs. 2 and 3). Inside

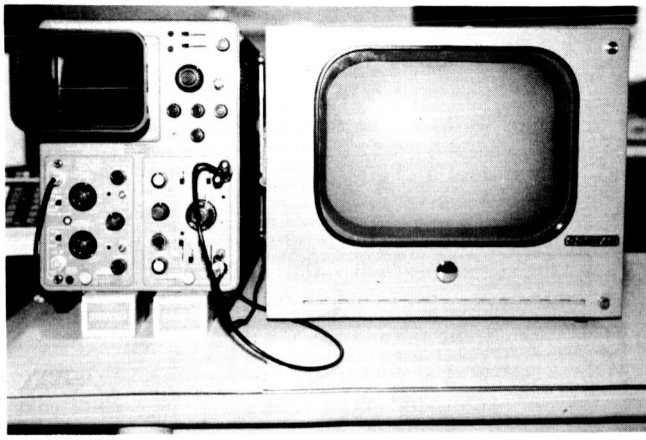

Fig. 1. Storage oscilloscope and slow-scan monitor

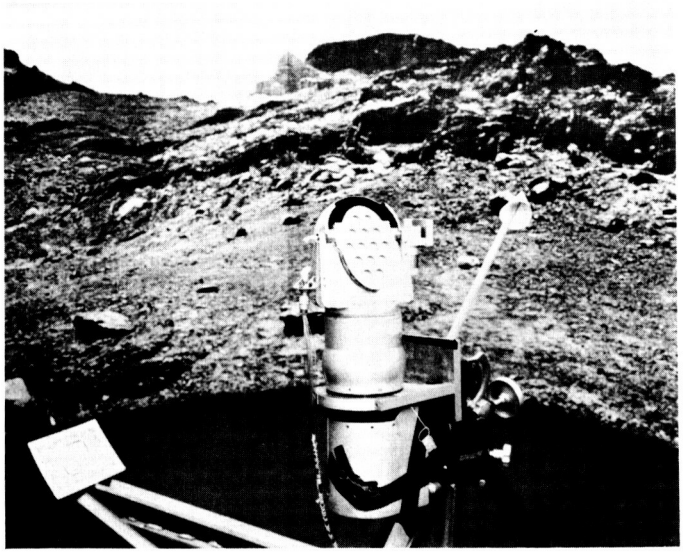

Fig. 2. Prototype *Surveyor* TV camera inside panorama

Fig. 3. Prototype *Surveyor* TV camera and panorama as viewed from top edge of panorama

is a photographic display of scenery illuminated by floodlamps. During the training exercises, the camera mirror is stepped in both azimuth and elevation, thereby simulating a real mission.

(3) The camera and mounting tripod are located on the roof of the JPL Space Flight Operations Facility. All operating functions of the TV camera are utilized. The only disadvantage of this configuration is the presence in the video data of distinguishable familiar items such as buildings and automobiles.

An important part of the training exercises is the simulation of malfunctions and anomalies with the TV camera. After a malfunction or anomaly is recognized by the TelPAC Group, corrective action is recommended so that a particular camera survey can continue and usable video data can be obtained. From the experience gained thus far while simulating many non-standard situations, sets of corrective action and failure flow diagrams for the following anomalies have been generated to aid in quickly obtaining a solution:

(1) Underexposed picture (above and at noise level).

(2) Saturated picture—overexposed.

(3) Shaded picture.

(4) Torn or noisy picture.

(5) Filter and iris interrogation sequences.

(6) Automatic and manual iris failures.

(7) Shutter failure.

(8) Focus failure.

(9) Mirror azimuth and elevation failures.

(10) Focal length failure.

(11) Filter wheel failure.

5. Future Plans

The training exercises are scheduled to continue using both standard and non-standard situations. The 4.2.2 camera is being modified to operate in an emergency mode as well as the new star integration mode. Since both of these are possible operating modes for the first *Surveyor* mission, both will be used with the 4.2.2 camera in future training exercises.

A tape recording was made of the video signal from the flight camera aboard the first flight spacecraft. A complete first survey was made with this camera during the recording. The playback of the video data will permit the TelPAC Group to become familiar with the flight camera data and to distinguish parts of the spacecraft within the camera's field of view.

B. Planetary Color Photography

Introduction. Observation indicates that a high proportion of planet reflectance is white light. Vivid sensations of color from objects illuminated by sunlight are essentially close-range phenomena. As range increases, coloring becomes diluted. Hence, interest for exploratory, long-range (50 to 5000 mi) planetary photography is directed at the reproduction of diluted color tones, i.e., tones that enter the white region or the grey region.

The reproduction of color requires a technology that involves the superposition of three primaries. With adequate spectral separation and accurate quantitative adjustment, any color in nature, including white, may be satisfactorily matched with three selected components. Only in special cases can a match be obtained when any one of the selected components is absent. For example, in the reproduction of fully saturated colors occupying a narrow band, two primaries may suffice.

Adequate spectral separation of the three primaries is secured by a selection from the red, green, and blue regions. A mixture of red and green light produces yellow. With the addition of a correctly proportioned quantity of blue light, a colorless sensation arises and is designated white. This phenomenon is demonstrated every day with the reception of compatible television color broadcasting.

Color in planetary photography. As with all other photography, planetary photography may be related to the Munsell system for defining color. In this system, color has three attributes: hue, saturation, and brightness. Saturation represents the intensity of the coloring or the extent to which the color is diluted with white.

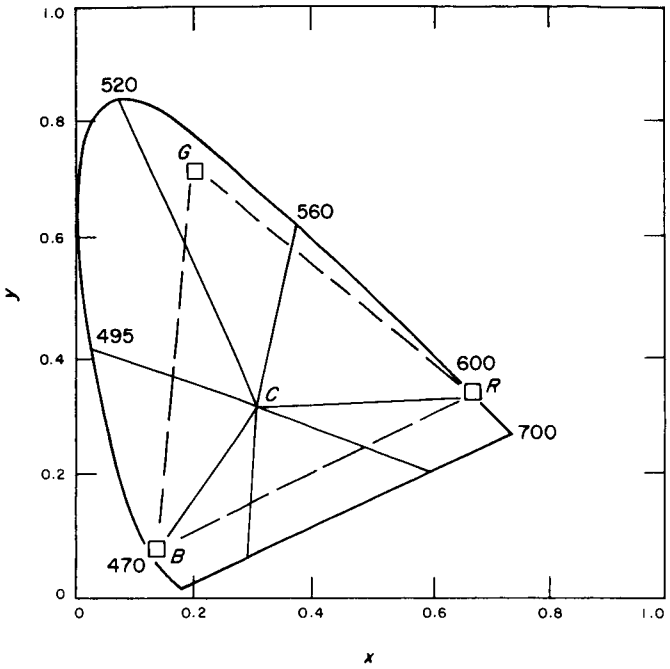

Fig. 4. NTSC color triangle in CIE coordinates

The relationship of white to colors is illustrated in the CIE[1] chromaticity diagram of Fig. 4. The curve represents the locus of fully saturated pure spectral colors. Nonspectral colors, or purples that are a mixture of red and blue, form the base of the color curve. Generally, the y ordinate is associated with luminance, and the x ordinate is associated with chromaticity. Greens tend to have high luminance, while reds and blues have progressively lower luminance. Inserted into this diagram is illuminant C, which represents north-sky daylight with coordinates $x = 0.3101$ and $y = 0.3163$. Illuminant C will be defined as white; i.e., when observed by the eye, no color sensation will be evoked.

The lines connecting C with the perimeter represent the degree of saturation for any particular color. The closer the chromatic coordinates are to C, the less intense is the saturation or the fainter is the hue. Colors of low saturation cannot be simulated unless all three primaries are present. Thus, although blue, for example, may not be observed as a distinctive shade, it is one of the three selected primaries that must be employed to produce a white contribution.

Because surfaces in nature tend to reflect a high proportion of the incident sunlight, planetary photography will naturally be concerned with colors of low saturation. The contribution of the white light to the hue thus becomes the predominating factor in spectral evaluations of planetary images taken from orbiting or flyby space vehicles.

NTSC compatible color TV system. The problems that have arisen in television color broadcasting with compatibility and bandwidth compression are of particular interest for planetary photography. The need to generate black and white luminance signals when broadcasting in color has stressed the property of luminance in electronic color reproduction.

Insofar as planetary photography is accomplished by electronic processes, advantage may be taken of the techniques that have been developed for color TV. A constant-luminance, trichromatic system is specified for TV color broadcasting by the National Television Systems Committee (NTSC). The video spectrum is divided into three channels of decreasing bandwidth that carry monochromatic, trichromatic, and bichromatic information. The final image is presented on a tricolor dot-mosaic picture tube. For the purposes of planetary photography, a chemical dye process must be added to produce the final color photograph.

NTSC defines three primaries in CIE coordinates as red $x = 0.67$, $y = 0.33$; green $x = 0.21$, $y = 0.71$; and blue $x = 0.14$, $y = 0.08$. From these three primaries, a luminance signal is specified $E_Y = 0.30E_R + 0.59E_G + 0.11E_B$. The assumption is made that, when reproducing the standard illumination source C, $E_Y = E_R = E_G = E_B$.

The NTSC primaries, as defined above, may be inserted into the CIE diagram to form a color triangle, as depicted in Fig. 4. The NTSC system reproduces all colors that are contained within the triangle. The color reproduction so obtained claims a wider chromatic range than the better commercial printing processes.

If the output signals from a color camera, i.e., three camera tubes having suitable color filters, is proportioned as indicated for E_Y, the signal may be reproduced monochromatically. When appropriate gamma corrections are made to linearize system parameters, the photometric functions, as opposed to chroma values, that are observed by the camera will be correctly evaluated. In this way, the equation for E_Y forms the basis of a compatible television system where the output from a color camera can be reproduced as a monochromatic picture on a black-and-white picture tube. This is illustrated in the simplified diagram of Fig. 5. The reverse process is also true

[1] International Commission on Illumination.

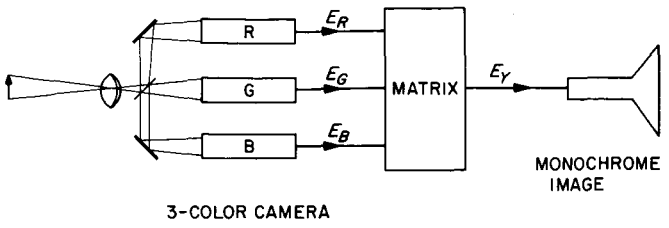

Fig. 5. Monochrome reproduction from three-color stimulus

where a monochrome camera produces a monochromatic picture on a tricolor picture tube.

Data reduction. A further interesting property of electronic color reproduction uncovered by NTSC research is that chromatic information can be inserted at greatly reduced resolution and that fine detail need be carried on a monochrome basis only. This is based on the property of the eye which has a limited resolution for chromatic detail. Thus, NTSC specifies a maximum video frequency of 4.2 Mc for monochrome information, while the trichromatic and bichromatic signals are limited to 1.3 Mc and 400 kc, respectively. The NTSC findings indicate that the data requirement for planetary color photography need not greatly exceed the monochrome requirement.

The NTSC chromatic information is transmitted as two additional signals designated I and Q. These are derived from the red-green-blue primaries

$$I = 0.59R - 0.27G - 0.32B$$

$$Q = 0.21R - 0.52G + 0.31B$$

At the receiver, by appropriate matrixing, three primary color signals R, G, B are derived from the Y and I, Q signals:

$$R = 0.96I + Y + 0.62Q$$

$$G = -0.27I + Y - 0.65Q$$

$$B = -1.11I + Y + 1.70Q$$

These represent three signals that are applied to the tricolor picture tube and form the basis of the compatible color and black and white reproduction.

Although there is no compatibility requirement for planetary photography, the ability to reproduce accurate monochrome information from only one of three sets of transmitted data could prove to be a valuable redundancy asset in space technology.

Camera filters. The spectral characteristics of the color filters required for the camera require a conversion from the CIE diagram into the RGB color triangle. The filter characteristics so obtained are

$$R, G, B = \frac{\alpha_{1,2,3}}{\alpha_1 + \beta_1 + \gamma_1}\bar{x} + \frac{\beta_{1,2,3}}{\alpha_1 + \beta_1 + \gamma_1}\bar{y}$$

$$+ \frac{\gamma_{1,2,3}}{\alpha_1 + \beta_1 + \gamma_1}\bar{z}$$

where $\bar{x}$, $\bar{y}$, and $\bar{z}$ are CIE tristimulus values, and α, β, and γ are functions of the x, y coordinates of the primaries. Typical filter characteristics are shown in Fig. 6.

Real-time transmission is not a requirement in exploratory planetary photography, and the chromaticity coordinates of each picture element, as derived from the transmitted camera signals, may be computer evaluated. This being the case, color signals may be sequentially generated instead of simultaneously generated as in broadcast TV. Thus, the need for three camera tubes is less apparent and depends more on the effective ground velocity of the planetary imaging device than on simultaneity.

Two-color system. When only two color filters are employed with a single camera, as in the *Mariner IV* TV system, a need arises for the insertion of a third primary if any attempt is to be made to reproduce tonal values throughout the visible spectrum. Photography of

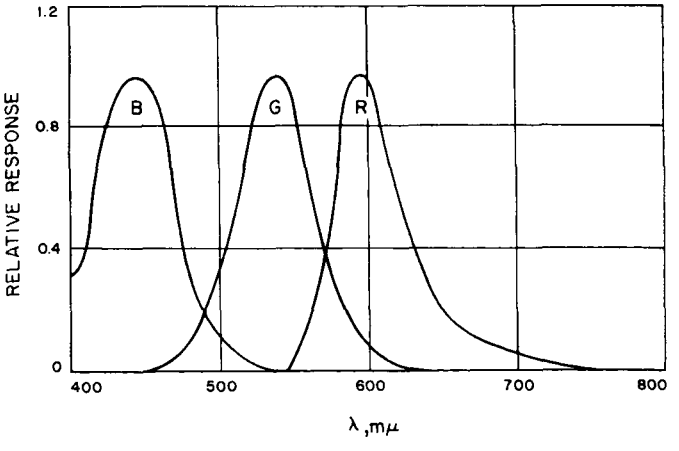

Fig. 6. Color filters employed in the NTSC camera system

Mars was accomplished with alternate green and red filters, with some degree of overlap in certain of the reproductions. In this case, a blue primary is required to permit presentation of a sufficiently wide range of tonal values at low saturation. One solution would be to include, as part of the chromatic information, direct observation from Earth. Although the direct observation is at lower resolution, as discussed above, high resolution is not necessarily a requirement for chromaticity insertion. A possibility thus arises of adding a synthetic blue primary in a quantity which will attempt to match tonal values with Earth observations.

Summary. Irrespective of apparent coloring, planetary color photography requires consideration of the entire visible spectrum. Because of compatibility and bandwidth compression, the NTSC system of color TV broadcasting is of particular interest. Components such as the tricolor picture tube may prove invaluable in the mechanization of ground systems.

VII. Physics

A. Total Radiation Dose Experienced by the *Mariner IV* Spacecraft as Measured by the Ion Chamber Experiment

The *Mariner IV* ion chamber experiment was performed to measure the spatial and temporal variations of galactic cosmic rays and to observe trapped particles and solar cosmic rays when encountered. This experiment was designed and built by Prof. H. V. Neher (California Institute of Technology), principal investigator; H. R. Anderson (JPL), coexperimenter; and L. G. Despain (JPL), cognizant engineer. A single Geiger-Müller (G-M) counter and an integrating ion chamber were used to measure the G-M tube counting rate (average omnidirectional flux of penetrating charged particles) and ionization rate produced by all radiation behind 0.010 in. of steel shielding. The shielding mass thickness was 0.2 g/cm^2, which is the range of 10-Mev protons. From the data obtained, the total radiation dose experienced by the *Mariner IV* spacecraft was estimated.[1] The three types of radiation to which the spacecraft was exposed are discussed below.

1. Galactic Cosmic Rays

Galactic cosmic rays consist of protons, alpha particles, and heavier nuclei, mostly with energies exceeding 200 Mev. Outside the Earth's atmosphere, their flux was constant within 10% for the first 230 days of the *Mariner IV* mission, as judged by terrestrial and Earth satellite measurements. The ion chamber experiment measured 4 particles/cm^2-sec and 1.7 mrads/hr$\simeq$1000 ion pairs/sec-cm^3 of air (standard temperature and pressure) from launch until March 17, 1965, at which time the ion chamber

[1] In assessing the effects of radiation upon the spacecraft, it must be remembered that by far the largest amount of energy absorbed by the surfaces facing the Sun is carried by the solar photon flux and the solar wind (consisting of 10^8 protons/cm^2-sec with an average energy of 1 kev). Their energy is absorbed by the first few microns of the sunward surfaces.

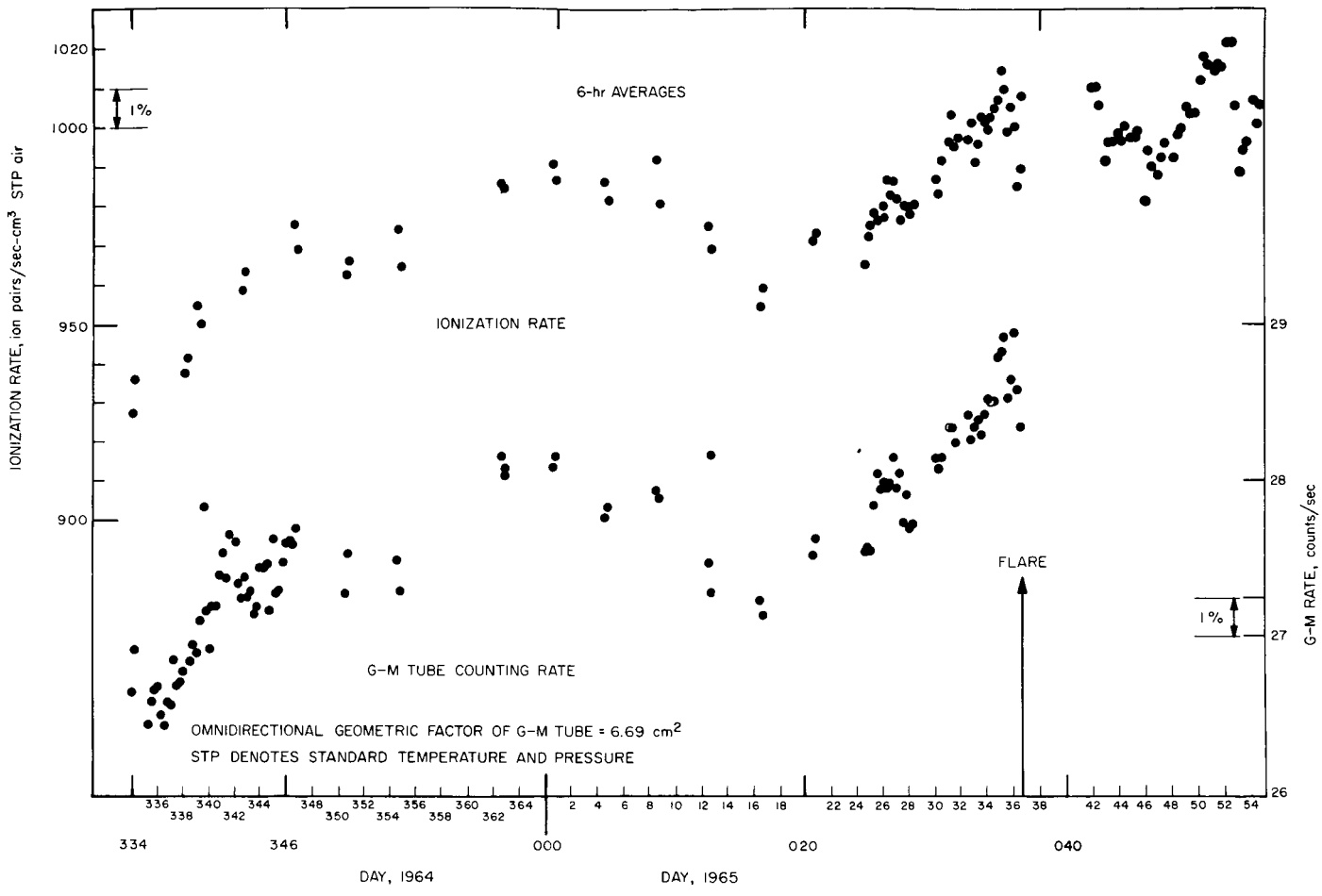

Fig. 1. 6-hr Averages of ionization rate and G-M tube counting rate for the first portion of the *Mariner IV* mission

ceased operating. In 230 days at these rates, the dose amounted to 7.9×10^7 particles/cm² and 9.5 rads. The 6-hr averages of these quantities for the first portion of the mission are shown in Fig. 1. Preliminary data were used; averages for all intervals have not been computed.

Because the radiation was penetrating, these doses were uniform within 20% throughout the spacecraft. The average specific ionization was about 5.5 Mev/(g/cm²), i.e., about three times the minimum ionization. There are large local fluctuations about this figure due to nuclear stars produced in the material of the spacecraft. As solar activity increases toward the maximum predicted for 1968 and 1969, the flux and ionization rate of galactic cosmic rays will gradually decrease by about a factor of 2.

2. *Solar Protons*

Almost all of the solar protons encountered by *Mariner IV* through March 17, 1965, occurred in the 2 days following a solar flare at 18:00 GMT on February 5. The counting and ionization rates measured by the ion chamber experiment during this period are shown in Fig. 2.[2] The total dose using 0.2-g/cm² shielding was 1.3×10^7 particles/cm² and 4.2 rads.

Unlike the galactic cosmic rays, the average energy from these particles (mostly protons according to data from the cosmic ray telescope)[3] was 30 to 40 Mev. Other measurements made near the Earth suggest that there are 3% as many particles above 80 Mev as there are above 10 Mev; hence, the dose diminished by a factor of

[2]The units in Fig. 2 may be converted using the following:

6.69 counts/sec = 1 particle/cm²-sec

579 ion pairs/sec-cm³ of air (standard temperature and pressure) = 1 mrad/hr

[3]Reported by Simpson, J. A., and O'Gallagher, J., American Geophysical Union Annual Meeting, Washington, D. C., April 1965.

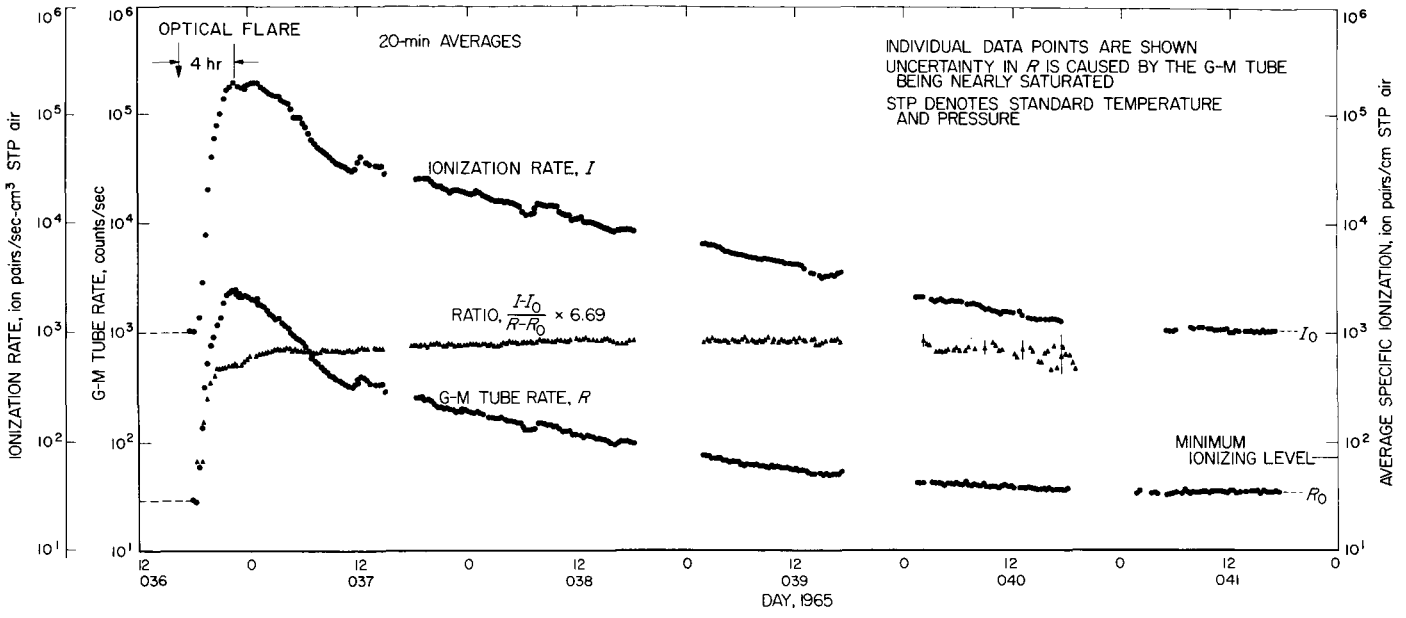

Fig. 2. 20-min Averages of ionization rate, true G-M tube counting rate, and average specific ionization for the period following the solar flare of February 5, 1965

approximately 30 in going from 0.2- to 7-g/cm² depth in the spacecraft. The number of protons with ranges between 0.001 and 0.2 g/cm² (0.5 to 10 Mev) was on the order of 10^5/cm², judging from preliminary trapped radiation detector data.[4]

The ion chamber has not functioned since March 17, but the other radiation detectors on the *Mariner IV* spacecraft have shown small fluxes of low-energy protons and electrons on several occasions. However, no significant flux of solar particles with ranges exceeding 0.2 g/cm² was encountered between March 17 and the beginning of picture playback on July 15.

3. *Trapped Particles at Earth*

The counting and ionization rates measured by the ion chamber experiment in the Earth's Van Allen radiation belts are shown in Fig. 3. The dose measured for the inner belt (mostly protons of energy from 10 to 100 Mev) using 0.2-g/cm² shielding was 0.36×10^7 particles/cm² and 1.9 rads. For the outer belt (mostly electrons of energy greater than 1 Mev), the dose measured was 13.4×10^7 particles/cm² and 8.2 rads. Thus, the total dose measured in the Van Allen radiation belts was 13.8×10^7 particles/cm² and 10.1 rads.

The particles trapped in the Earth's radiation belts are mostly of low energy. Thus, the number of particles having ranges between 0.001 and 0.2 g/cm² was on the order of 100 times greater than the numbers given, while the number of particles reaching 3 g/cm² or greater must have been on the order of 100 times less. No trapped particles were observed in the vicinity of Mars.

B. *Mariner IV* Magnetic Measurements Inside the Earth's Magnetosphere, Magnetic Tail, and Magnetosheath[5]

Preliminary scientific results of the *Mariner IV* magnetic measurements are presented here, based on an analysis of the magnetometer data obtained as *Mariner*

[4] Reported by Van Allen, J. A., Frank, L., and Krimigis, S. M., American Geophysical Union Annual Meeting, Washington, D. C., April 1965.

[5] Excerpted from a paper presented at the Sixth International Space Science (COSPAR) Symposium, Mar del Plata, Argentina, May 1965. Coleman, P. J., Jr., Smith, E. J., Davis, L., Jr., and Jones, D. E., "Measurements of Magnetic Fields in the Vicinity of the Magnetosphere and in Interplanetary Space: Preliminary Results from *Mariner IV*," submitted for publication in *Space Research*, Vol. VI.

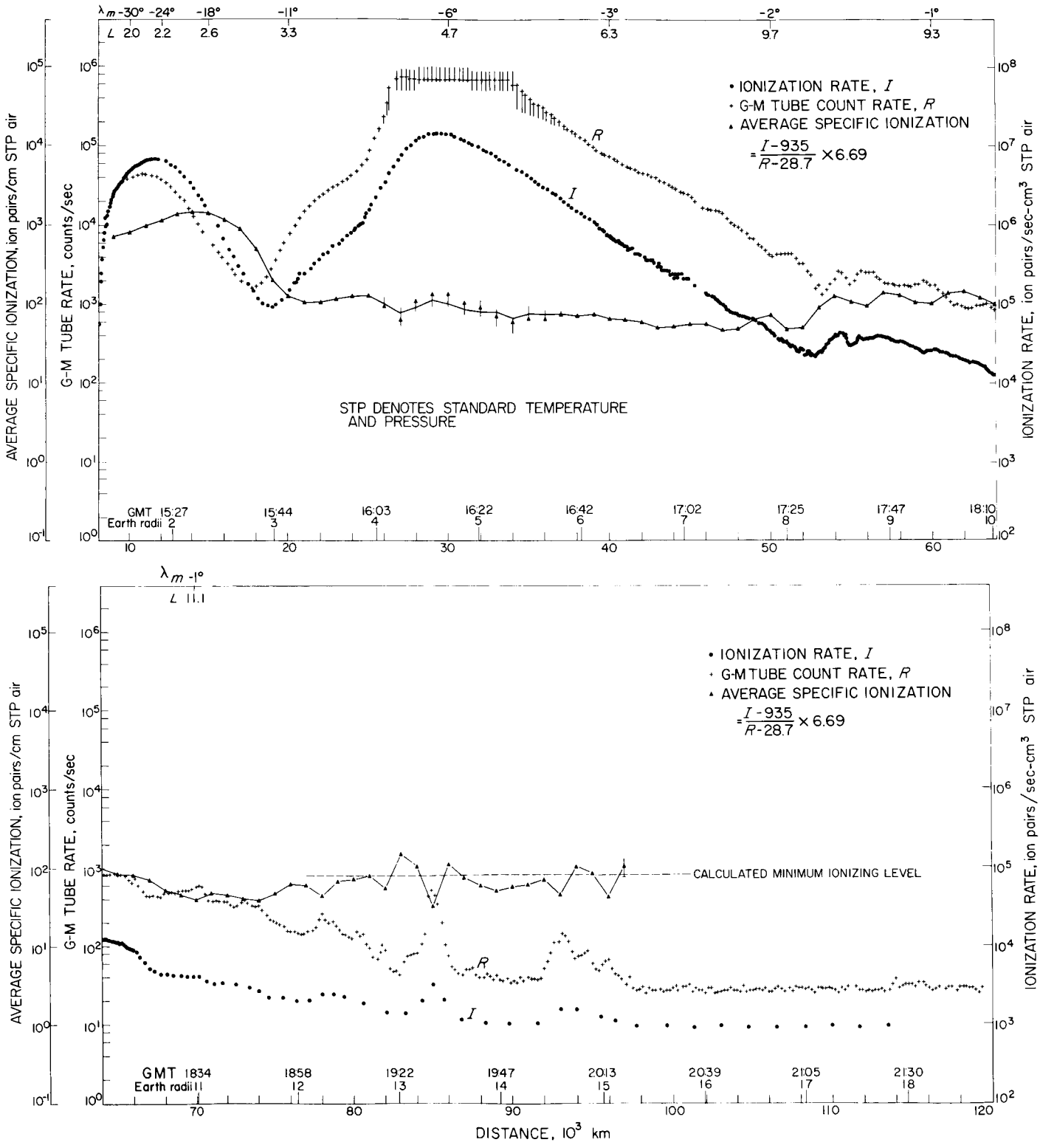

Fig. 3. Ionization rate, true G-M tube counting rate, and average specific ionization in the Earth's Van Allen radiation belts

IV passed outward through the Earth's magnetosphere and crossed the transition region and the hydromagnetic bow shock.

1. Low-Field Vector Helium Magnetometer

The *Mariner IV* magnetometer, a new type of instrument never before flown on spacecraft, was developed for use on missions requiring a wide range of operating temperature, an extended dynamic range (a necessity if a substantial planetary field may be encountered), good absolute accuracy, and high sensitivity (a necessity to the study of interplanetary magnetic fields during the flight to the planet and to the search for small perturbations of the interplanetary field if the planetary field is weak). Fields as large as 625 γ (± 360 γ referred to any of the three components; 1 $\gamma = 10^{-5}$ gauss) may be measured, with a limiting noise threshold equivalent to an rms field of 0.1 γ. The instrument sensitivity (16.7-mv output for 1.0 γ of applied field) is linear to within 0.1% over the full range. This is one aspect of the absolute accuracy which is ensured by the stability of both the linear characteristic and the null point (output voltage in the absence of an ambient field) over both an extended temperature range (-25 to 65°C) and long periods of time. High absolute accuracy is an important requirement for an instrument flown on an attitude-stabilized spacecraft, whereas, on a spinning spacecraft, the spin permits an inflight determination of the zero-field outputs of instruments measuring field components transverse to the spin axis.

When the *Mariner* Mars 1964 Project was initiated, the above specifications equaled or exceeded those of the more conventional fluxgate or second-harmonic type of magnetometer such as that utilized on the *Mariner II* spacecraft (Ref. 1). The weight and power requirements of the two kinds of instruments were comparable. Furthermore, it was felt that the *Mariner IV* magnetometer would be able to satisfy the stringent reliability requirements of the planetary mission.

Like the rubidium magnetometer (Ref. 2) and the high-field scalar helium magnetometer (Ref. 3), the low-field vector helium magnetometer for *Mariner IV* is a resonance magnetometer in which a specimen gas is examined spectroscopically, using optical pumping to detect changes in state caused by the presence of weak magnetic fields. However, unlike the others, the low-field vector helium magnetometer is not an absolute instrument producing tones, the frequencies of which are proportional to the field magnitude. Instead, it generates three steady or DC voltages, each of which is proportional to a component of the ambient field.

A simplified schematic diagram of the *Mariner IV* magnetometer is shown in Fig. 4. The pumping light, 1.08-μ radiation obtained from an electrodeless discharge helium lamp, is circularly polarized and focused on a helium absorption cell, where it is partially absorbed by metastable helium atoms. Absorption and pumping are observed by an infrared (IR) lead sulfide detector. Since simple Zeeman absorption depends on both the polarization of the resonant radiation and its direction of incidence with regard to the magnetic field, the pumped condition can be destroyed by changing the direction of the magnetic field. When a rotating field is applied to the cell, it causes a periodic variation in the transparency of the gas. A sweep oscillator produces two sinusoidal currents 90 deg out of phase in two mutually perpendicular sets of Helmholtz coils (represented in Fig. 4 by a circle) placed around the absorption cell. This generates a 100-γ field rotating at a rate of 50 rev/sec. Empirically, it is found that the absorption is proportional to the square of the cosine of the angle between the light beam (optical axis) and the magnetic field. Thus, in the absence of an ambient field, the detector output is a second harmonic of the sweep frequency. If the DC field is present, the detector output contains a component at the sweep frequency whose phase depends on the angle between the optical axis of the sensor and the DC field. The AC amplifier passes a signal containing only the fundamental frequency component, which is used to generate, by phase-coherent detection, a DC current that is applied to the Helmholtz coils to null the external field. Therefore, the magnetometer functions as a closed-loop or feedback system, with a resulting improvement in output linearity and stability.

Fig. 4 shows the electronics for a two-axis system. The triaxial *Mariner IV* instrument utilizes a time-sharing technique to switch the plane of the sweep vector on alternate rotations from the plane of the diagram to a plane perpendicular to the diagram through the optical axis. This commutation provides essentially simultaneous triaxial measurements when the outputs are sampled at *Mariner IV* data rates.

A photograph of the *Mariner IV* magnetometer is shown in Fig. 5. The triaxial Helmholtz coils lie on a 4-in.-D sphere, with the helium lamp and igniter at one end and the detector and preamplifier at the other. The weight of the sensor (Fig. 5, right side) is 1 lb, and that of the two

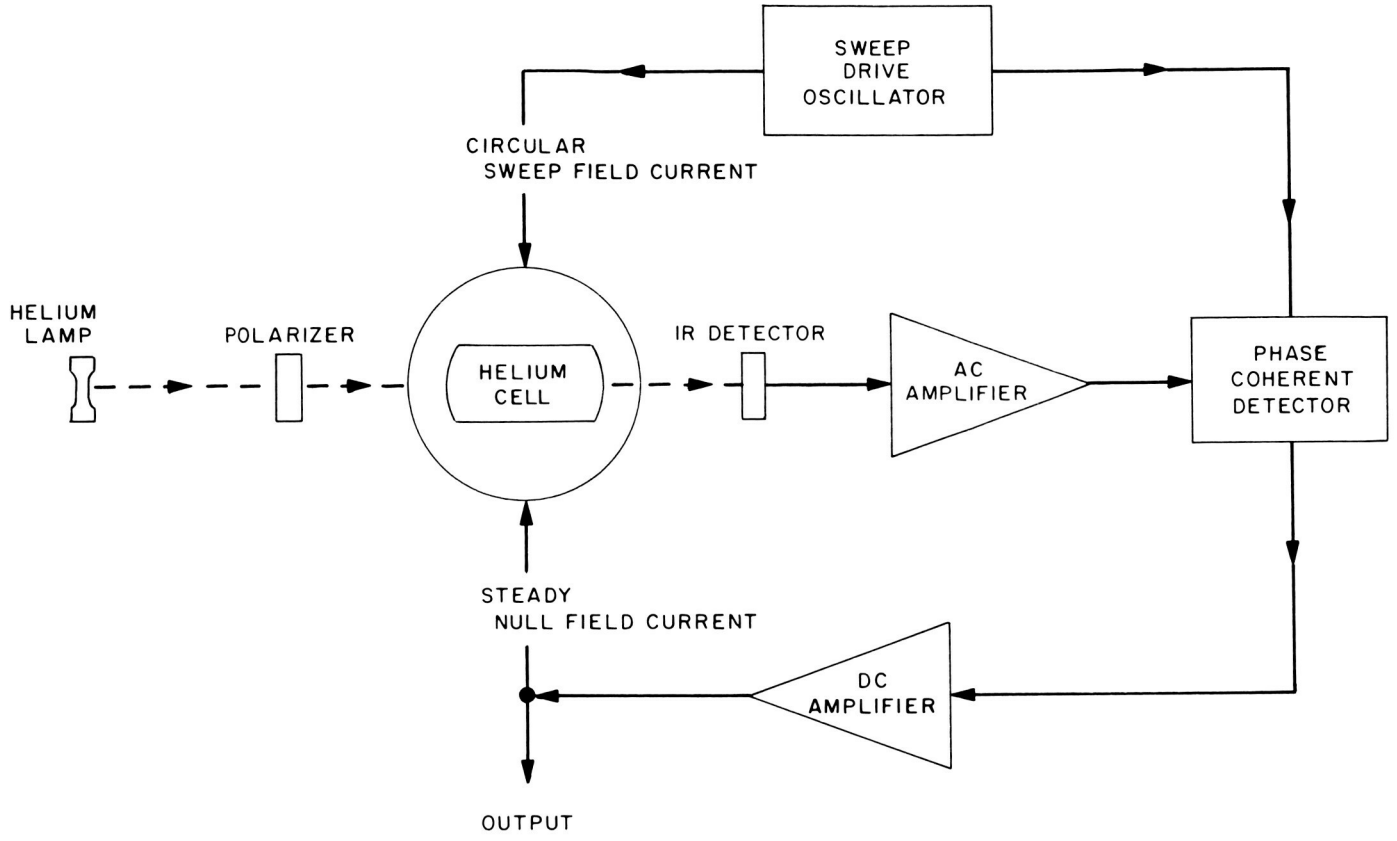

Fig. 4. *Mariner IV* magnetometer schematic diagram

modules containing the rest of the electronics (Fig. 5, left side) is 4.5 lb.

2. Near-Earth Data

The 10-min averages of the total field magnitude $|B|$ and the magnitude of the solar radial component $|B_r|$ are given in Fig. 6 as functions of GMT or, alternatively, geocentric distance. During this time interval, which began shortly after the magnetometer came on scale and ended just prior to complete attitude stabilization, *Mariner IV* rotated slowly (approximately 2 rev/hr) about an axis oriented toward the Sun. The changing orientation, relative to the ambient field, of the two sensor axes transverse to the Sun-oriented axis allowed the corresponding components of the spacecraft field to be derived. The value of $|B_r|$ was adjusted to agree with the radial component of the unperturbed geomagnetic field near the Earth. The three spacecraft field components, which total 28 γ at the sensor, were subtracted from the data before $|B|$ was computed.

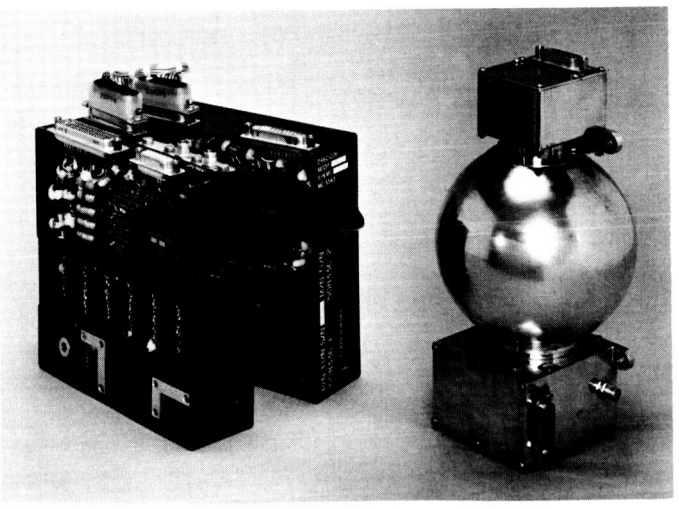

Fig. 5. *Mariner IV* magnetometer

The data show four distinctly different magnetic regimes separated by transitions designated in Fig. 6 as 1, 2, and 3. The data from nearest the Earth to the first transition (at approximately 12 Earth radii) show the

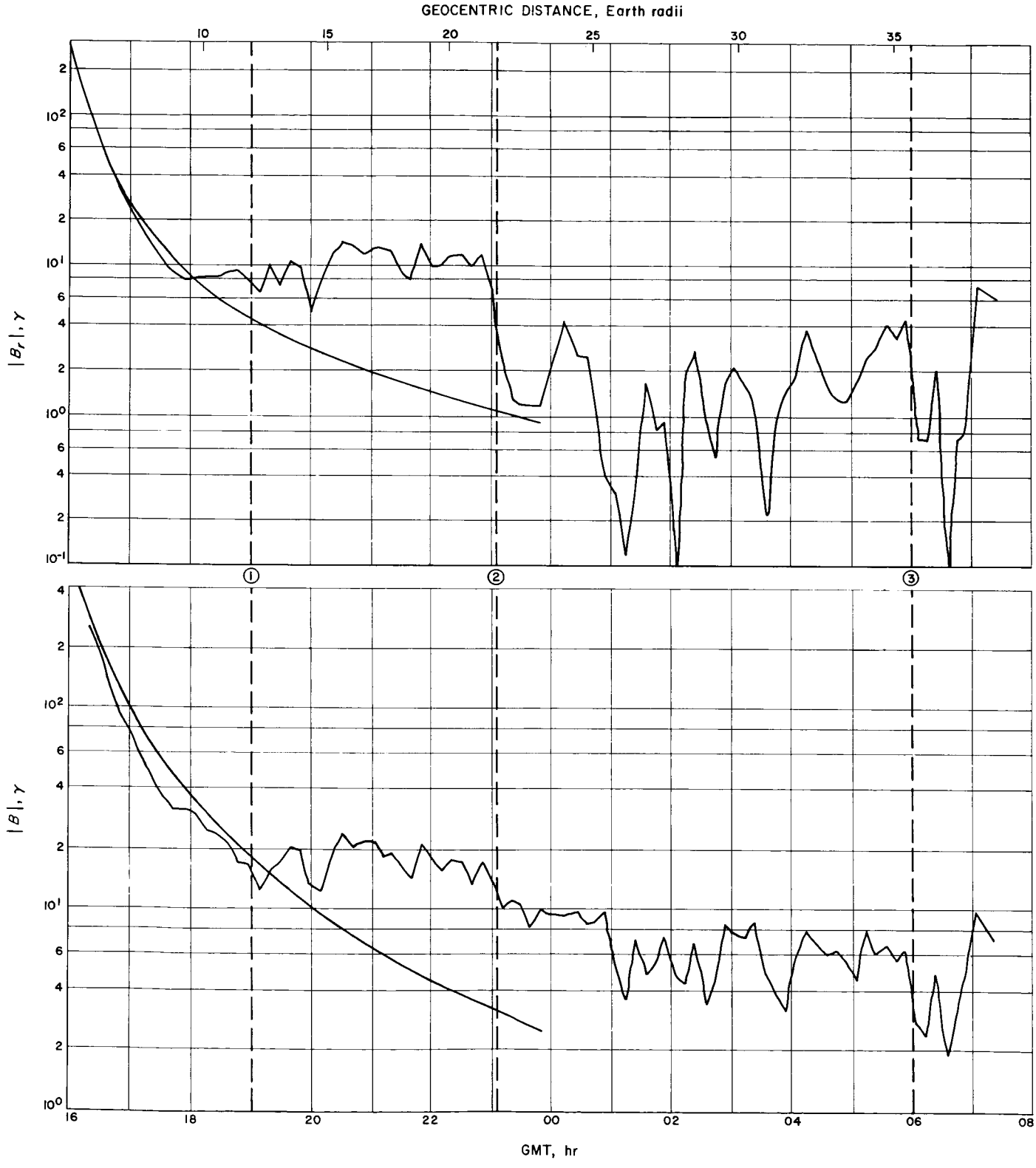

Fig. 6. *Mariner IV* magnetometer data acquired near Earth

same general dependence on geocentric distance as the unperturbed geomagnetic field. The average field from Transition 1 to Transition 2 (at approximately 22 Earth radii) is essentially constant in magnitude, with an enhanced radial component that points away from the Sun (no directional information given in Fig. 6). The smaller (5- to 10-γ) average field in the region between Transitions 2 and 3 is irregular in magnitude and direction. Transition 3 (at approximately 35 Earth radii), not completely obvious in the 10-min averages, marks the edge of a zone in which regions of rapidly fluctuating fields alternate with regions of relatively stable fields (discussed below).

The locations of the three major transitions along the *Mariner IV* trajectory and the relationship of these transitions to the different regions of interaction between the solar wind and the magnetosphere are illustrated in the top half of Fig. 7. Shown are the asymmetric magnetosphere, consisting of a torus formed by field lines that co-rotate with the Earth; an elongated magnetic tail pointing away from the Sun (Ref. 4); and the detached hydromagnetic bow shock (Ref. 5). Transition 1 is identified with the boundary between the co-rotating magnetosphere and the tail; Transition 2, with the boundary between the tail and the turbulent magnetosheath; and Transition 3, with the so-called standing shock front. These boundary locations agree reasonably well with corresponding transitions in the *Mariner IV* plasma and energetic particle data, as well as with previous field and particle measurements by other spacecraft.

The bottom half of Fig. 7 is essentially a polar plot of the near-Earth trajectory, and is not a simple projection into a fixed plane such as the ecliptic. The dashed curves show the average location of the magnetopause and shock front as derived from *IMP-1 (Interplanetary Monitoring Probe 1)* magnetometer data (Ref. 6). Transition 3 occurs near the extension of the outer contour. Transition 2 lies beyond the inner contour, but is generally consistent with the spread in the individual boundary penetrations by *Explorer 10* (Ref. 7), *Explorer 14* (Ref. 8), and *IMP-1* (Ref. 6) at approximately the same Sun–Earth–spacecraft angle. The innermost transition detected by the *Mariner IV* magnetometer appears to be associated with the general feature in the distribution of trapped electrons with energies greater than 40 kev. Omnidirectional flux contours obtained by the *Explorer 14* instruments (Ref. 9) show a bifurcation behind the dawn line, at an average geocentric distance of approximately 9 Earth radii, that is quite likely associated with the change from the magnetosphere proper to the magnetic tail. Detailed comparisons now in progress suggest that the large scale characteristics of the fields observed by *Mariner IV* in the different regions also agree with those of earlier measurements made by *Explorers 10* and *14* and *IMP-1*.

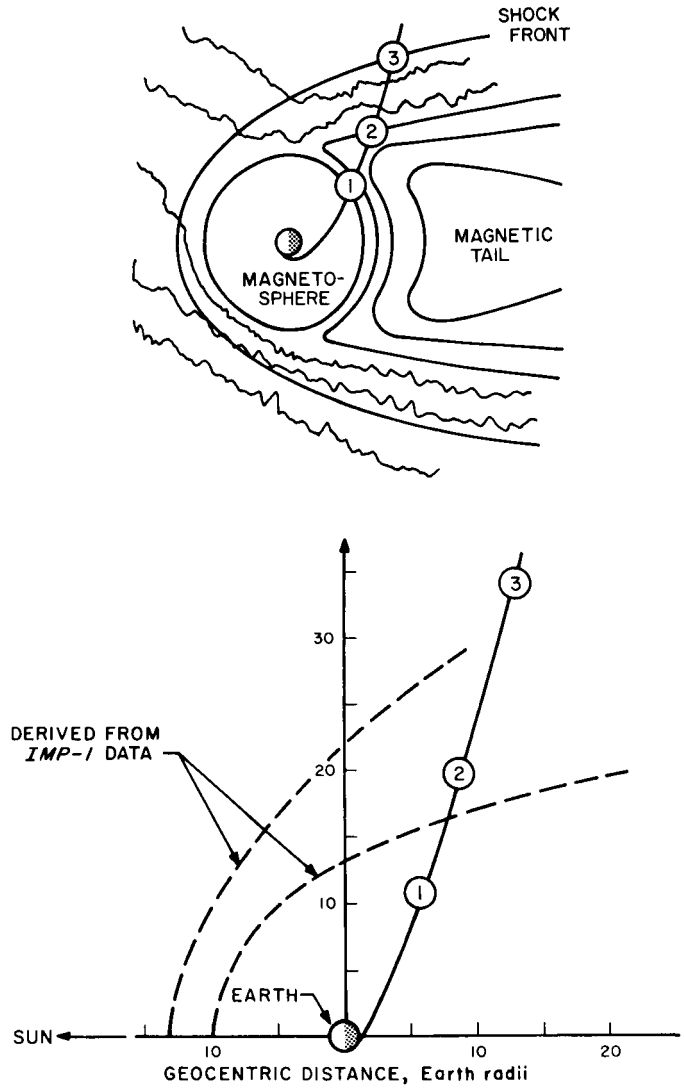

Fig. 7. *Mariner IV* near-Earth trajectory

The data acquired beyond Transition 3 merit special attention because the important features are associated with the fine structure of the field, which is obscured by averaging. Fig. 8 is a plot of all the magnetic measurements made during a 1-hr interval corresponding to the range of geocentric distances between 36 and 38 Earth radii. The radial field component B_r is parallel to the axis of *Mariner IV*, which was continuously pointed at the Sun. The spacecraft was rolling about the Z-axis at a gyro-controlled rate, causing sinusoidal variations to appear in the two transverse field components B_X and B_Y.

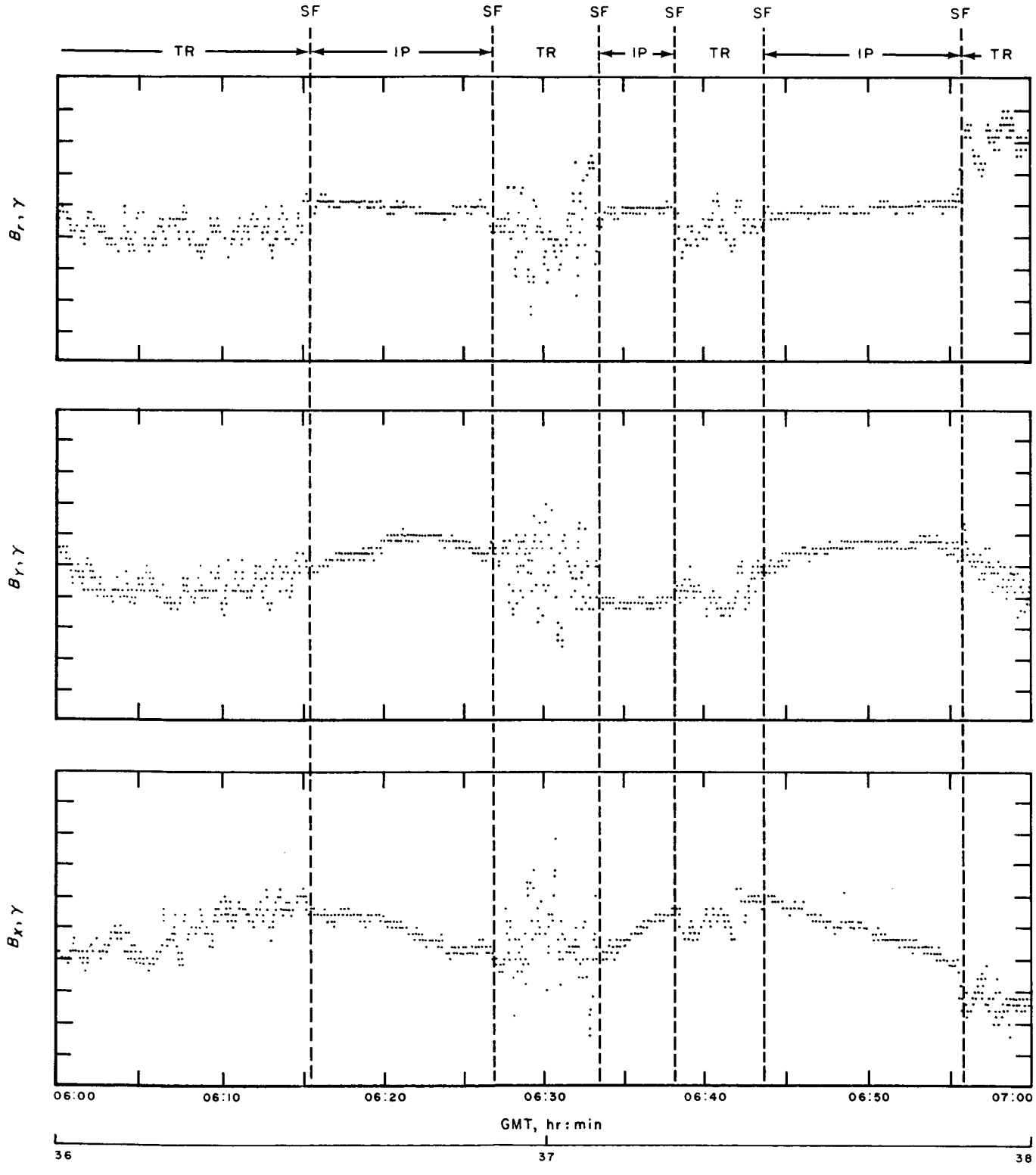

Fig. 8. *Mariner IV* magnetometer data showing multiple passages of the shock front

No attempt was made to remove the effect of the spacecraft roll which caused the variations with periods of approximately 30 min. Vertical lines corresponding to the instantaneous shock front (SF) position divide the data in Fig. 8 into intervals when *Mariner IV* was inside the transition region (TR) and outside the shock in the interplanetary (IP) medium. The four triaxial measurements, each 12.6 sec, reveal regions of higher noise levels that alternate with regions of relative quiet. The last such observation came at 07:18 GMT and is not shown.

We identify the abrupt changes from the transition region to interplanetary space with successive passages through the shock front. This interpretation is supported by the *Mariner IV* plasma measurements, which show penetrations into the free-streaming solar wind to be coincident with several of the shock front transitions in the magnetometer data. The multiple passages through the shock front suggest that it is not stationary, but surges back and forth over distances of several Earth radii with typical periods of 5 to 20 min, at least for this time and location. These results seem quite reasonable, as it has been suggested that hydromagnetic shocks resemble hydraulic phenomena in which irregular and fluctuating fronts with considerable structure and precursors ahead of the main shock are typical. The sharp nature of most of the observed transitions suggests that the shock front makes a large angle with the trajectory and moves a considerable distance, rather than suggesting that the trajectory lies nearly tangent to the front. Presumably, it is the unknown velocity of motion of the front, and not the known velocity of the spacecraft, that determines the apparent duration of the crossing from one region to the other. The average interval between successive observations of the shock is comparable to the time required for the solar wind to slide around the magnetosphere; thus, it is not clear whether the local variations in the position of the front are caused by fine structure in the solar wind or by some form of instability.

The outstanding feature of the magnetic data is the occurrence of irregular fields behind the shock with or without an accompanying change in average field magnitude. The same feature was used to identify the *IMP-1* shock front locations (Ref. 6) and is also obvious in the *OGO-1* (*Orbiting Geophysical Observatory 1*) search coil magnetometer data[6]. The fluctuations inside are very roughly five times as great as those outside the front. Preliminary inspection of tabulated data indicates that periods of 10 sec or more are prominent in the fluctuations in the transition region and that periods of 2 to 4 sec or shorter are much less important. Since the field must be convected with the solar wind velocity, the length scale of the irregularities should be of the order of $10^{3.5}$ km. There is also a noticeable oscillation (not shown in Fig. 8) with a period of 2 or 3 min (which corresponds to a length of the order of the magnetopause radius of curvature) and an amplitude of several γ.

[6] McLeod, M., Holzer, R. E., and Smith, E. J., "Preliminary *OGO-1* Search Coil Magnetometer Results," 1965 (In press).

References

1. Smith, E. J., Davis, L., Jr., Coleman, P. J., Jr., and Sonett, C. P., "Magnetic Measurements Near Venus," *Journal of Geophysical Research*, Vol. 70, p. 1571, 1965.
2. Ruddock, D. A., "Optically Pumped Rubidium Vapor Magnetometer for Space Experiments," *Space Research*, Vol. 2, p. 692, 1961.
3. Keyser, A. R., Rice, J. A., and Schearer, D. L., "Metastable Helium Magnetometer for Observing Small Magnetic Fluctuations," *Journal of Geophysical Research*, Vol. 66, p. 4163, 1961.
4. Axford, W. I., Petschek, H. E., and Siscoe, G. L., "Tail of the Magnetosphere," *Journal of Geophysical Research*, Vol. 70, p. 1231, 1965.

References (Cont'd)

5. Spreiter, J. R., and Jones, W. P., "On the Effect of a Weak Interplanetary Magnetic Field," *Journal of Geophysical Research,* Vol. 68, p. 3555, 1963.

6. Ness, N. F., Scearce, C. S., and Seek, J. B., "Initial Results of the *IMP-1* Magnetic Field Experiment," *Journal of Geophysical Research,* Vol. 69, p. 3531, 1964.

7. Heppner, J. P., Ness, N. F., Skillman, T. L., and Scearce, C. S., "*Explorer X* Magnetic Field Measurements," *Journal of Geophysical Research,* Vol. 68, p. 1, 1963.

8. Cahill, L., "Preliminary Results of the Magnetic Field Measurements in the Tail of a Geomagnetic Cavity," *Transactions of the American Geophysical Union,* Vol. 45, p. 231, 1964.

9. Frank, L. A., Van Allen, J. A., and Macagno, E., "Charged Particle Observations in the Earth's Outer Magnetosphere, *Journal of Geophysical Research,* Vol. 68, p. 3543, 1963.